Electronic Supporting Information (ESI)

For

Direct observation of humic acid-promoted hydrolysis of phytate through stabilizing a conserved catalytic domain in phytase

Xinfei Ge[a], Wenjun Zhang[a,*], Christine V. Putnis [b,c], and Lijun Wang[a]

[a]College of Resources and Environment, Huazhong Agricultural University, Wuhan 430070, China

[b]Institut für Mineralogie, University of Münster, 48149 Münster, Germany

[c]School of Molecular and Life Science, Curtin University, Perth 6845, Australia

Number of pages: 44

Number of tables: 7

Number of figures: 56

SI Experimental Section

Preparations of HA stock solution

10 g HA sodium salt (Sigma-Aldrich, code H16752) was dissolved in 1 L ultrahigh purity water to obtain 10 g/L HA solution that was adjusted to pH 5 as the stock solution. No particles were observed on bare or organically-coated mica surfaces at the concentrations of HA ranging from 0.01 to 1 mg/L for nucleation experiments, whereas the aggregation of HA particles occurred on relevant surfaces with increasing HA to 50 mg/L, which was used for PF-QNM measurements. Due to the much larger characteristic differences of HA from different natural soils,[1] the experimental results obtained from these HA are not generalizable. Therefore, the purchased HA from Sigma Aldrich that is considered an international standard material was used to explore the generalizability of results.

Organically-coated muscovite mica surface preparations. Muscovite mica was selected as a model mineral due to its atomically flat surface (001).[2] Prior to modification, mica was pretreated by using adhesive tape to get a clean surface. In order to form more silanol groups (Si-OH), the freshly cleaved micas were placed in a 120 ℃ oven for 2 h.[3] Subsequently, micas were moved into a clean petri dish to prevent surface contamination and dried in a stream of nitrogen (N_2) for at least 30 min at room temperature. Silanol self-assembled thin films terminated with -OH or -COOH functional groups were coated on pretreated mica surfaces as models of organo-coatings representing soil organic interfaces such as polysaccharides and

organic acids widely present in soil rhizospheres.[4,5] Then, the pretreated micas were immersed in toluene with 20 wt % silanol-terminated polydimethylsiloxane (as -OH precursor) or 20 wt % (3-Triethoxysilyl) propyl succinic anhydride (Gelest) (as -COOH precursor) for 24 h.[6] The organically-coated micas were rinsed with acetone and water in sequence to remove the loosely attached organics and finally stored in water until use. After functionalization, the silanol head groups of these two precursor chemicals covalently bonded to the mica surfaces through Si-O-Si,[7] leaving functional groups of -OH or -COOH exposed to solution (Fig. S2). The successful functionalization was verified by the existence of Raman characteristic peaks of -OH and -COOH, respectively (Fig. S3).

***In situ* AFM experiments**

a. AFM imaging of nucleation involving hydrolysis product

In situ nucleation experiments on bare or organically-coated surfaces of mica were conducted in a 100 μL liquid cell by a Multimode 8 AFM (Bruker, Santa Barbara, CA). The nucleation images were collected at a scan rate of 1.95 Hz with samples/line 256 with commercially available ScanAsyst-Fluid+ (spring constant 0.7 N/m and tip radius 2 nm) in ScanAsyst mode at 25 ℃ on different nucleation surfaces, including bare, -OH- and -COOH-coated mica. Phytase was dissolved in phosphate buffer saline (PBS) solution and stored in an ultra-cold refrigerator at −80℃ for using. Prior to each nucleation experiment, the fresh solutions (1mg/L phytase, 20 μM phytate, pH

5 and *IS* = 10 mM) with 1 mM $CaCl_2$ and different concentrations of HA ranging from 0.01 to 1 mg/L or with 1 mM $FeCl_3$ and 1 mg/L HA were prepared in order to avoid homogeneous nucleation in bulk solutions. And pH values and ionic strengths (*IS*) of all prepared solutions in nucleation experiment were adjusted by stock solution of sodium hydroxide or hydrochloric acid (0.1 M) and sodium chloride (1 M), respectively. The newly-prepared solutions were pumped into the liquid cell using a high-precision syringe pump at a constant rate of 10 mL/h to ensure steady-state kinetic nucleation conditions rather than diffusion-controlled nucleation conditions over a period of nucleation experiments.[8] Prior to each nucleation experiment, the height distributions of different nucleation surfaces in solutions of pH 5 and *IS* = 10 mM were obtained to ensure that nucleated particles are not artifact, and therefore the number of particles can be accurately determined without interference from the roughness of different nucleation surfaces of mica (Fig. S3). The solution condition of pH 5 and *IS* = 10 mM was optimal for enzymatic activity obtained from phytase activity experiments (Fig. S4A-B). Furthermore, the control experiments (Fig. S5-S34) were performed to confirm that observed particles were not HA, phytase or phytate aggregates at low concentrations of HA (≤ 1 mg/L) in the absence and presence of 1 mM Ca^{2+} in solutions of pH 5 and *IS* = 10 mM. During the 30-minute nucleation, the nucleation rates on different nucleation surfaces were determined according to number of nuclei in the absence and presence of HA ranging from 0.01 to 1 mg/L, respectively.

b. Tip Decoration. The detailed tip decoration procedures have been reported previously.[8] Prior to decoration, the bare SNL-10 probes (Bruker, CA) were treated under UV/ozone for 10 min, followed by immersion into acetone for 30 min, then rinsed by ethanol and water several times and finally dried under a nitrogen (N_2) stream. Cleaned tips were coated with gold (Au) by an ion sputter instrument (model JFC-1600, JEOL, Japan) and rinsed again into acetone, ethanol, and water. The Au-coated probes were then immersed for 40 min in a N, N-dimethylformamide (DMF) solution containing 0.2 mM of heterobifunctional cross-linker LC-SPDP consisting of a pyridyl disulfide,[9,10] which covalently adsorbed on Au-coated tips through an oxidation addition to the gold surface, and an N-hydroxysuccinimide (NHS) ester that reacts with N-terminal amine of these two domains by the formation of a stable amide bond. After rinsing with DMF, followed by ethanol to remove the unbound cross-linker, the probes were dipped into PBS containing 50 nM ACD/FLP overnight. Functionalized tips were stored in water until use.

c. PeakForce Quantitative Nanomechanical Mapping (PF-QNM). Prior to PeakForce-QNM measurements, the HA particles were deposited on bare or organically-coated surfaces of mica. AFM images of surface topography and adhesion force were obtained simultaneously in the solution of pH 5 and *IS* 10 mM by using functionalized-tips under the mode of PeakForce-QNM in a liquid cell at a constant rate of 0.997 Hz and a resolution of 256 × 256 pixels to explore the binding strengths of ACD/FLP to HA. At the beginning and end of each measurement, the inverse

optical lever sensitivity (InvOLS) of the functionalized cantilever were detected through the laser deflection method[11] and then the thermal calibration method[12] was utilized to calibrate spring constant of each cantilever of the modified tips. To account for the affinity of ACD or FLP with HA under different solution conditions, at least 100 force-distance curves between ACD/FLP and HA were extracted from AFM images of adhesion force.

Phytase Activity and Stability.

a. Preparations of Color Reagents. Reagents for color reaction were prepared according to a previous method.[13] Reagent A: sulfuric acid (5 N). Dilute 70 ml concentrated sulfuric acid (95-98%, GR) to 500 ml. Reagent B: ascorbic acid (0.1 M). Dissolve 1.32 g of ascorbic acid (MW 176.12, AR) in 75 ml of water. Because of easily oxidization, the solution should be prepared without light. Reagent C: ammonium molybdate (4 %). Dissolve 20 g ammonium molybdate (MW 1235.86, AR) in water and dilute to 500 ml. And store the solution in a brown bottle. Reagent D: potassium antimony tartrate (1 mg Sb/ml). Dissolve 0.2743 g of potassium antimony tartrate (MW 333.93, CP) in 100 ml of water. Reagent E: mixed reagent. The color reagent was prepared by mixing thoroughly 125 ml of 5 N sulfuric acid, 37.5 ml of ammonium molybdate, 75 ml of ascorbic acid and 12.5 ml of potassium antimony tartrate solution.

b. Determination of P_i Standard Curve. Accurately weigh 0.4390 g of potassium

dihydrogen phosphate (KH_2PO_4, Sigma-Aldrich) dried in an oven at 80 ℃ for 2 h. Dissolve it with water, add 5 ml of concentrated sulfuric acid and water to 1000 ml constant volume. Finally, the standard reserve solution containing 100 mg Pi /L was obtained. A series of standard solutions containing 0.0, 0.2, 0.6, 1.0, 2.0, 3.0, 4.0, 5.0 mg P_i/L were prepared by diluting the standard reserve solution. All standard solutions were adjusted to neutral conditions using 2, 4-dinitrophenol indicator (MW 184.11, AR) by dropping potassium hydroxide solution (50%, Sigma-Aldrich) or dilute sulfuric acid, respectively. Then, add 4 ml of color reagent and dilute to 25 ml in colorimetric tube. After 30 min at room temperature, the absorbance was measured by using UV spectrophotometer (UV1800ENG240, SOFT, SHIMADZU, Japan) at λ = 880 nm.

c. Orthophosphate Determination. Before the determination of phytate-released inorganic phosphorus, the blank measurements were performed to eliminate the interference of P_i contained in chemical reagent used (Table S2) and only minor impurities of P_i existing in phytate were detected within error. Thus, the concentrations of reactants involved in enzymatic hydrolysis reaction were determined. The enzymatic hydrolysis, containing 100 mg/L phytase, 20 μM phytate, various concentrations of HA ranging from 0.01 to 1 mg/L, different *IS* (1, 10, 100 mM) and pH (3, 5, 7, 9), occurred in 10 ml of reaction volume. All of enzyme assays were carried out at 25 ℃ for 30 min before being stopped by the addition of an acidic solution of 15% trichloroacetic acid (MW 163.38, AR). Subsequently, the reacted

solutions were treated with molybdenum blue method. Finally, the concentration of P_i (Table S3, S4) hydrolyzed by phytase was determined according to the standard curve under different solution conditions. In order to visually compare the changes of phytase activity under different solution conditions, concentration of P_i produced by enzymatic hydrolysis under pH 5 and *IS* = 10 mM in the absence of HA was taken as the standard P_i concentration and the phytase activity can be considered as relative activity, defined as concentrations of P_i produced under different solution conditions divided by standard P_i concentration, as a function of HA concentration at a given solution conditions. Prior to assays of phytase stability, 100 mg/L phytase solutions of pH 5 and *IS* = 10 mM containing various concentrations of HA ranging from 0.01 to 1 mg/L were incubated in colorimetric tube at 25 ℃ for 0, 2, 4, 6 and 8 h, respectively. The solution of pH 5 and *IS* = 10 mM, the optimal condition for phytase obtained from enzyme activity experiments (Fig. S4A, B), was selected for performing the experiments of phytase stability. After incubation, the amount of P_i by HA-incubated phytase can be determined (Table S5) according to the standard curve. Then, phytase stability can be defined as relative activity of free and HA-incubated phytase as a function of time.

Raman spectroscopy

A confocal Raman microscope (Horiba LabRAM HR800) was employed to quantitatively characterize secondary structures of ACD and full-length/mutant

phytase molecules in PBS solution (pH 5; *IS* 10 mM), and identify nucleated particles and organic-coated mica surfaces. The nucleated particles on mica after nucleation experiments were ultrasonically separated to be removed from mica substrates and further concentrated using a 5810R bench freezing centrifuge (Eppendorf, Germany). The enriched particles and the organic-coated surfaces of mica were characterized by Raman spectroscopy (Horiba HR800, France) following calibration by the characteristic band of silicon at 520.7 cm^{-1} using a laser of 532 nm with a 50 μm confocal hole, a 600 lines/mm grating and a 50 × microscope objective (Olympus, MLPlanTL N). The newly-cleaved mica was immersed into solutions containing 100 mg/L ACD or full-length/mutant phytase with and without 1 mg/L HA at pH 5 and *IS* 10 mM, and then the Raman spectra of secondary structure of protein before and after binding with HA under the same Raman operational parameters mentioned above were collected twice to decrease the single noise. The LabSpec 6 software was used to quantitatively analyze the protein secondary structure through Raman band-narrowing and curve-fitting of the protein spectral regions.[14,15]

The detailed Raman peak assignments of secondary structure of phytase and amide acid residues were listed in Table S1. During the band fitting, the line type for baseline correction of each spectrum was used and then the raw data after addition of Raman peaks of Amide I, II and III was fitted several times with Gauss-Lorentz function until χ^2 approached 1 as much as possible. After fitting, we can obtain the peak area of each fitted secondary structure to conduct quantitative analyses. The peak

intensity ratio of each fitted secondary structure including ordered α-helix, β-sheet and unordered conformation can be calculated through dividing the corresponding peak area by the total peak area. All calculated data are presented as mean values ± standard error (n = 3).

Table S1. Raman peak assignments of secondary structure of protein and amide acid residues.

Assignments	Unordered	α-helix	β-sheet
Amide I	1667 ± 3	1647 ± 1	1654 ± 2
Amide II	1560 ± 4	1545 ± 3	1551 ± 2
Amide III	1266 ± 3	1300 ± 8	1232 ± 4
C-C stretch (ring)	1600 ± 1		
CH_2 scissors	1456 ± 8		
C-O symmetric stretch	1410 ± 3		
CH_3 symmetric deformation	1369 ± 5		
CH_3 symmetric bend	1337 ± 6		

Table S2. Concentrations of P_i (mg P_i/L) in the solutions of pH 5 and IS = 10 mM with different reactants in the absence and presence of HA ranging from 0.01 to 1 mg/L.

c(HA)	Concentrations of Pi (mg Pi/L) with different reactants		
mg/L	None	Phytate	Phytase
0	0	0.011±0.008	0
0.01	0	0.012±0.007	0
0.1	0	0.008±0.004	0
1	0	0.011±0.005	0

Table S3. Concentrations of P_i (mg P_i/L) in the solutions of IS = 10 mM with different

pH values in the absence and presence of HA ranging from 0.01 to 1 mg/L.

c(HA) (mg/L)	Concentrations of Pi (mg Pi/L) under different pH values			
	3	5	7	9
0	0.331±0.012	0.654±0.012	0.413±0.011	0.139±0.007
0.01	0.413±0.014	0.830±0.010	0.470±0.014	0.191±0.010
0.1	0.516±0.028	0.928±0.013	0.553±0.012	0.252±0.009
1	0.583±0.012	1.018±0.010	0.658±0.014	0.375±0.018

Table S4. Concentrations of P_i (mg P_i/L) in the solutions of pH 5 under different *IS* values in the absence and presence of HA ranging from 0.01 to 1 mg/L.

c(HA) (mg/L)	Concentrations of Pi (mg Pi/L) under different *IS* values		
	1 mM	10 mM	100 mM
0	0.618±0.007	0.654±0.012	0.600±0.007
0.01	0.694±0.009	0.830±0.010	0.643±0.012
0.1	0.782±0.010	0.928±0.013	0.700±0.011
1	0.890±0.009	1.018±0.010	0.800±0.010

Table S5. Concentrations of P_i (mg P_i/L) in the solutions of pH 5 and *IS* = 10 mM with different incubation times in the absence and presence of HA ranging from 0.01 to 1 mg/L.

c(HA) (mg/L)	Concentrations of Pi (mg Pi/L) with different incubation time				
	0 h	2 h	4 h	6 h	8 h
0	0.654±0.012	0.518±0.007	0.348±0.010	0.225±0.018	0.114±0.008
0.01	0.830±0.010	0.671±0.009	0.470±0.014	0.336±0.007	0.287±0.009
0.1	0.928±0.013	0.792±0.009	0.643±0.009	0.583±0.012	0.545±0.009
1	1.018±0.010	0.924±0.009	0.817±0.010	0.767±0.012	0.740±0.009

Table S6. ACP nucleation rates (per 4 $\mu m^2 \cdot min$) on different surfaces of mica in the absence and presence of HA ranging from 0.01 to 1 mg/L.

c(HA) mg/L	Nucleation rates (per 4 μm^2·min) on different surfaces of mica		
	Bare	-OH-coated	-COOH-coated
0	3±0.13	8±0.28	11±0.48
0.01	6±0.20	12±0.53	15±0.59
0.1	9±0.17	16±1.00	18±0.85
1	11±0.22	20±0.90	26±0.71

Table S7. AIP nucleation rates (per 4 μm^2·min) on different surfaces of mica in the absence and presence of HA ranging from 0.01 to 1 mg/L.

c(HA) mg/L	Nucleation rates (per 4 μm^2·min) on different surfaces of mica		
	Bare	-OH-coated	-COOH-coated
0	3±0.13	8±0.28	11±0.48
0.01	6±0.20	12±0.53	15±0.59
0.1	9±0.17	16±1.00	18±0.85
1	11±0.22	20±0.90	26±0.71

Full-length phytase (FLP):

MSDMKSGNIS **RHGVRAP**PFL SLLIPLTPQS AFAQSEPELK

LESVVIVSMK AILITKATQL MQDVTPDAWP TWPVKLGWLT

PRGGELIAYL GHYQRQRLVA DGLLTKKGCP QPGQVAIIAD

VDERTRKTGE AFAAGLAPDC AISVHTQADT SSPDPLFNPL

KTGVCQLDNA NVTDAILSRA GGSIADFTGH RQTAFRELER

VLNFPQSNLC LNREKQDESC SLTQALPSEL KVSADNVSLT

GAVSLASMLT EIFLLQ**HD**QG MPEPGGEGSP IHTSGTPC

Mutant/recombinant phytase:

MSDMKSGNIS PFLSLLIPLT PQSAFAQSEP ELKLESVVIV

SMKAILITKA TQLMQDVTPD AWPTWPVKLG WLTPRGGELI

AYLGHYQRQR LVADGLLTKK GCPQPGQVAI IADVDERTRK

TGEAFAAGLA PDCAISVHTQ ADTSSPDPLF NPLKTGVCQL

DNANVTDAIL SRAGGSIADF TGHRQTAFRE LERVLNFPQS

NLCLNREKQD ESCSLTQALP SELKVSADNV SLTGAVSLAS

MLTEIFLLQQ GMPEPGGEGS PIHTSGTPC

Fig. S1. Amino acid sequences of FLP (Origin: EC 3.1.3.26, *Escherichia coli*) and mutant/recombinant phytase without N-terminal (RHGVRAP, ACD-1) and C-terminal (HD) active domains.

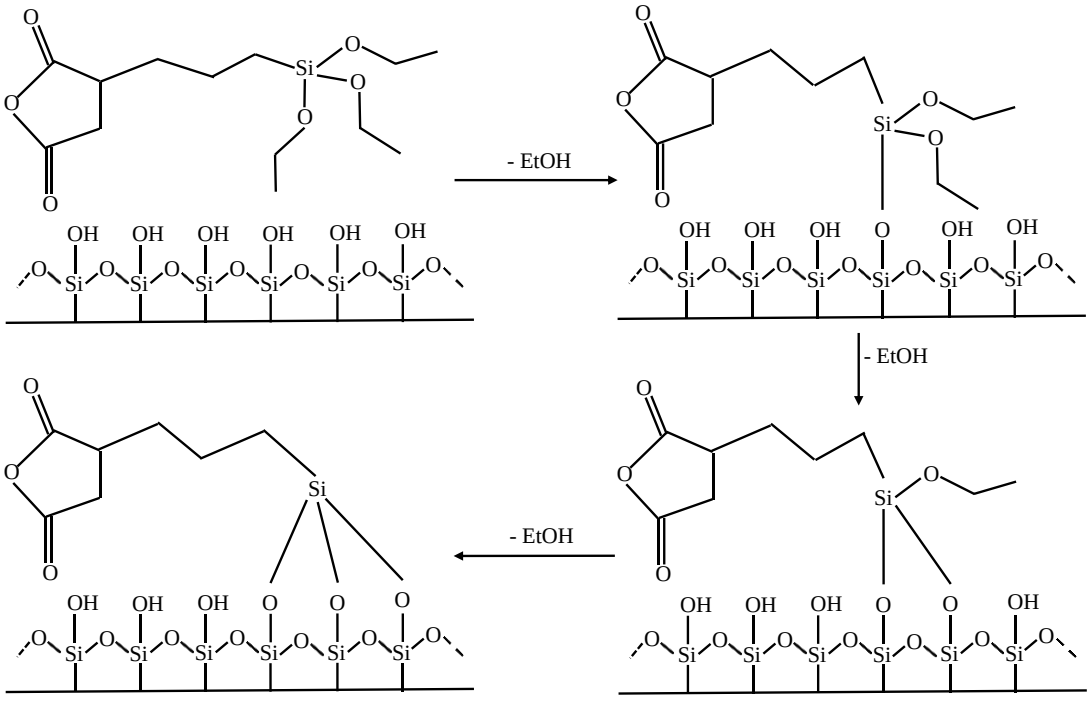

Fig. S2. Schematic for the reaction of precursor chemicals with mica. The precursor chemicals terminated with -COOH and –OH, respectively, react with hydroxy groups formed spontaneously on the pretreated mica surface.

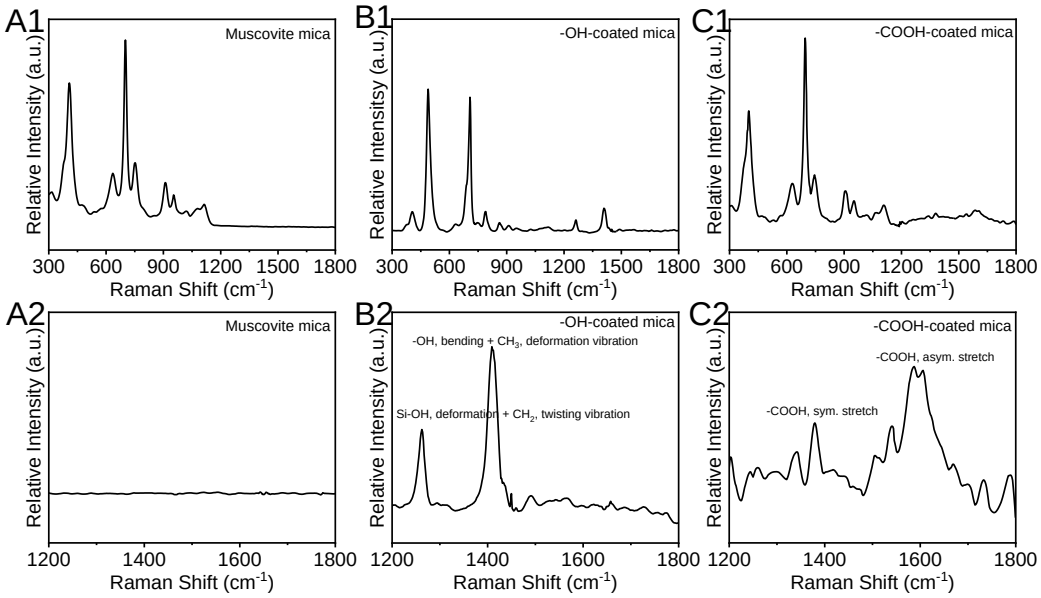

Fig. S3. (A1-C1) Raman spectra with the (A2-C2) corresponding magnified regions in 1200-1800 cm^{-1} of bare and organically-coated mica showing that the two precursor chemicals terminated with -OH and -COOH, respectively, firmly bond to the mica surface.

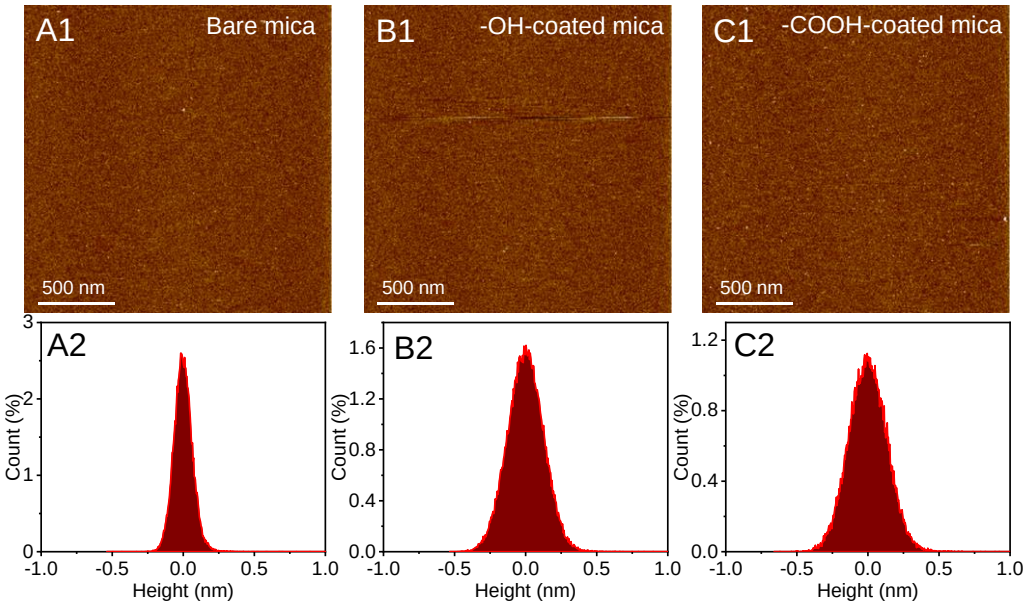

Fig. S4. AFM height images of (A) bare, (B) -OH- and (C) -COOH-coated surfaces of

mica, showing all the surfaces used for nucleation are atomically smooth.

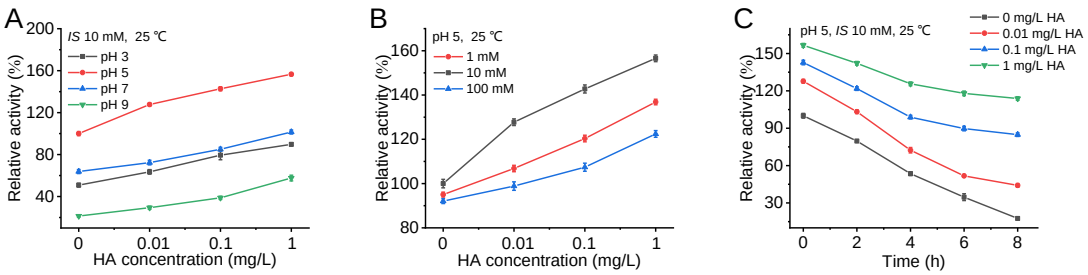

Fig. S5. The relative activity of phytase as a function of different concentrations of HA (0, 0.01, 0.1, 1 mg/L) at (A) pH values (3, 5, 7 and 9) and *IS* of 10 mM; (B) The relative activity of phytase at different *IS* of 1, 10 and 100 mM and constant pH 5. (C) The phytase relative activity at pH 5 and *IS* = 10 mM as a function of different incubation times in the absence and presence of HA ranging from 0.01 to 1 mg/L. The relative activity of phytase as a function of time was defined as the stability of phytase. Additionally, 100 mg/L phytase solution was diluted from the stock solution to make a solution at pH 5 and *IS* = 10 mM in the absence of HA and this solution was taken as the standard solution for the calculation of phytase relative activity. All assays were conducted at 25 ℃.

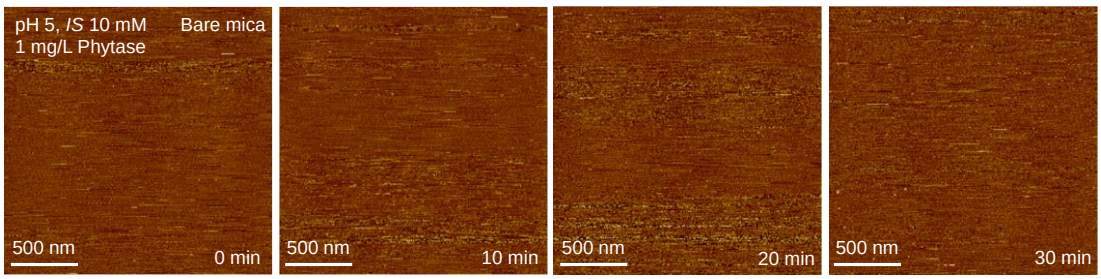

Fig. S6. No particles can be observed under the conditions of pH 5, *IS* = 10 mM containing 1 mg/L phytase on a surface of bare mica.

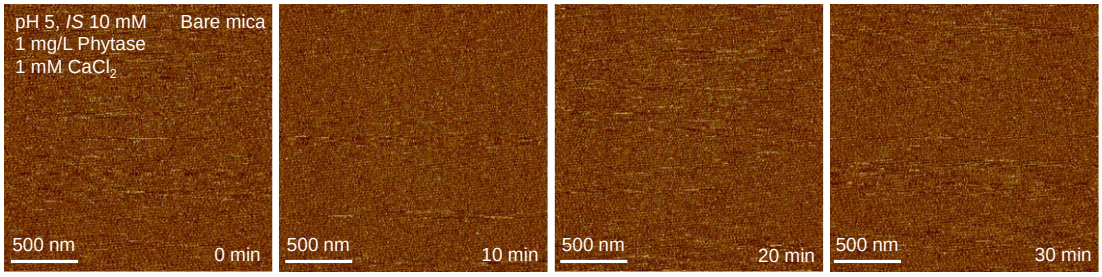

Fig. S7. No particles can be observed under the conditions of pH 5, *IS* = 10 mM containing 1 mg/L phytase and 1 mM $CaCl_2$ on bare mica.

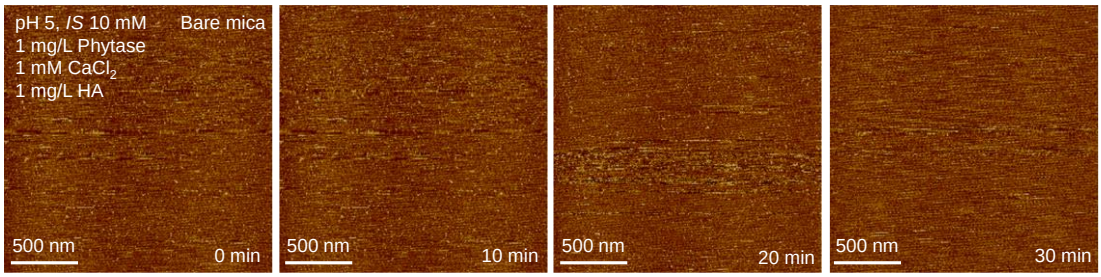

Fig. S8. No particles can be observed under the conditions of pH 5, *IS* = 10 mM containing 1 mg/L phytase, 1 mM $CaCl_2$ and 1 mg/L HA on bare mica.

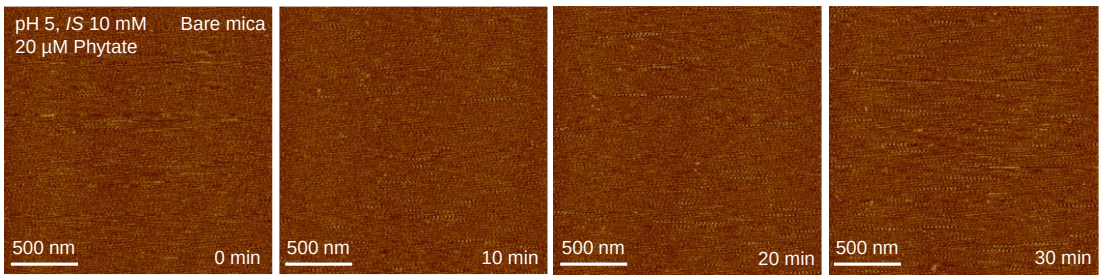

Fig. S9. No particles can be observed under the conditions of pH 5, *IS* = 10 mM containing 20 µM phytate on bare mica.

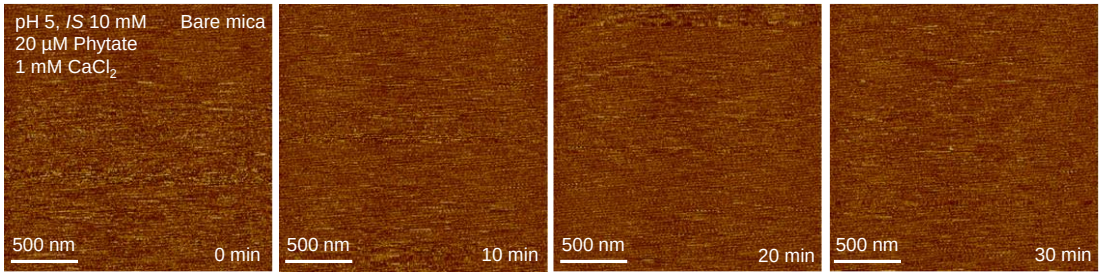

Fig. S10. No particles can be observed under the conditions of pH 5, *IS* = 10 mM containing 20 µM phytate and 1 mM $CaCl_2$ on bare mica.

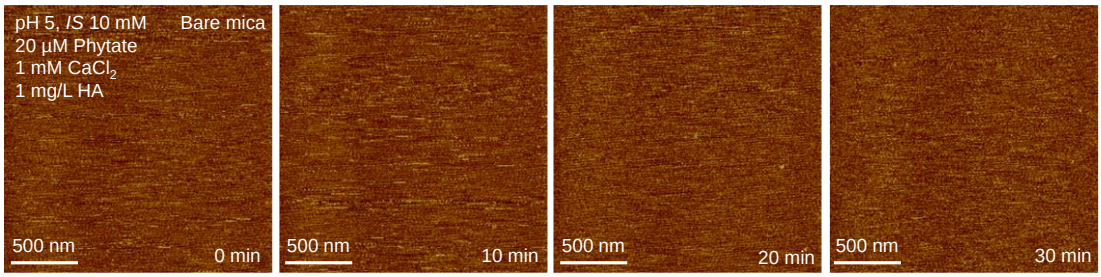

Fig. S11. No particles can be observed under the conditions of pH 5, *IS* = 10 mM containing 20 µM phytate, 1 mM $CaCl_2$ and 1 mg/L HA on bare mica.

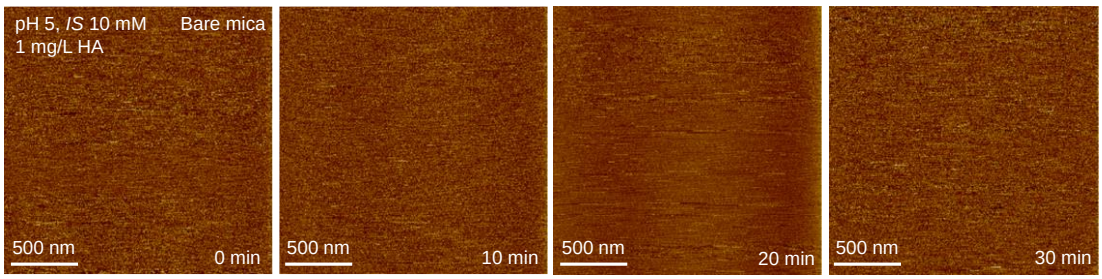

Fig. S12. No particles can be observed under the conditions of pH 5, *IS* = 10 mM containing 1 mg/L HA on bare mica.

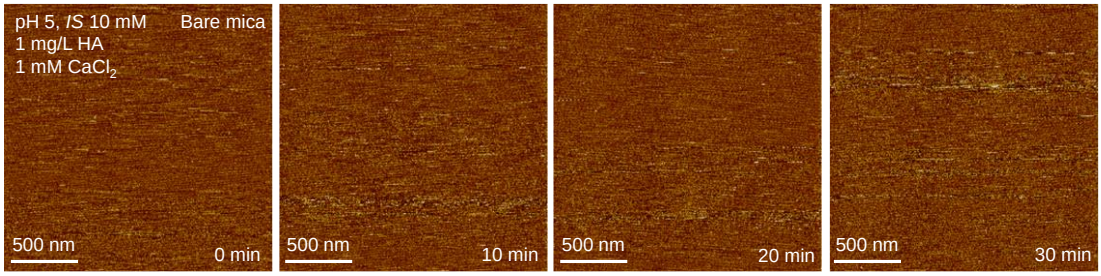

Fig. S13. No particles can be observed under the conditions of pH 5, *IS* = 10 mM containing 1 mg/L HA and 1 mM $CaCl_2$ on bare mica.

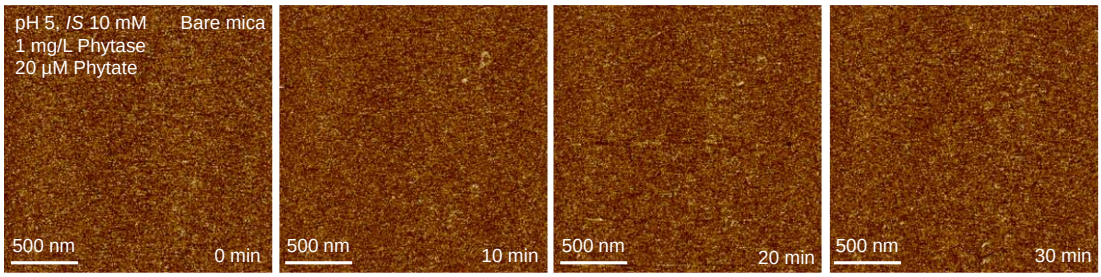

Fig. S14. No particles can be observed under the conditions of pH 5, *IS* = 10 mM containing 1 mg/L phytase and 20 µM Phytate on bare mica.

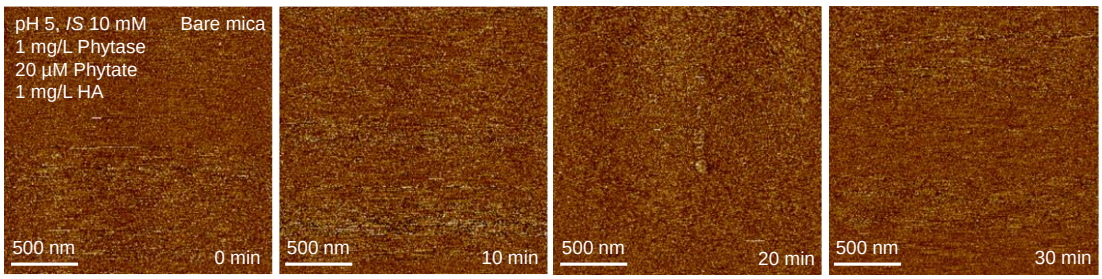

Fig. S15. No particles can be observed under the conditions of pH 5, *IS* = 10 mM containing 1 mg/L phytase, 20 µM phytate and 1 mg/L HA on bare mica.

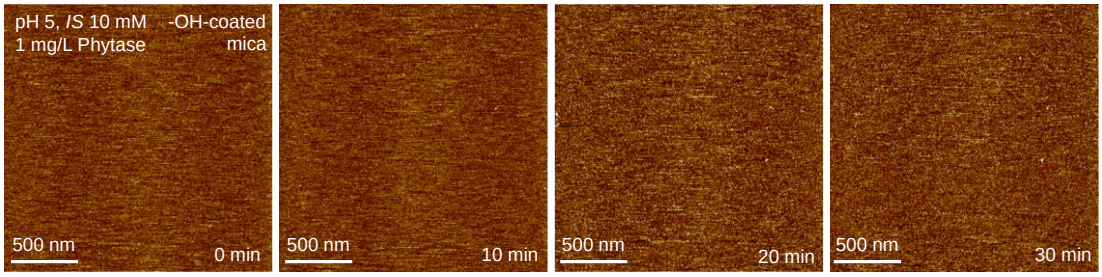

Fig. S16. No particles can be observed under the conditions of pH 5, *IS* = 10 mM containing 1 mg/L phytase on the -OH-coated mica.

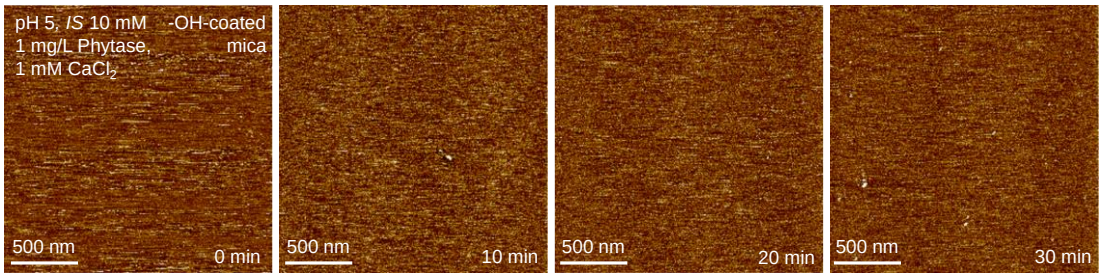

Fig. S17. No particles can be observed under the conditions of pH 5, *IS* = 10 mM containing 1 mg/L phytase and 1 mM $CaCl_2$ on the -OH-coated mica.

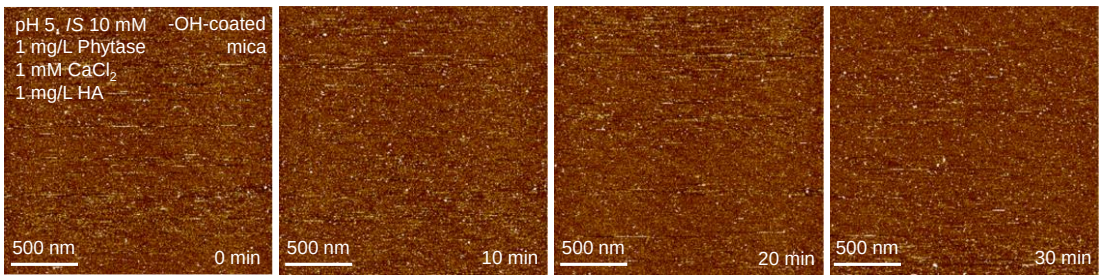

Fig. S18. No particles can be observed under the conditions of pH 5, *IS* = 10 mM containing 1 mg/L phytase, 1 mM $CaCl_2$ and 1 mg/L HA on the -OH-coated mica.

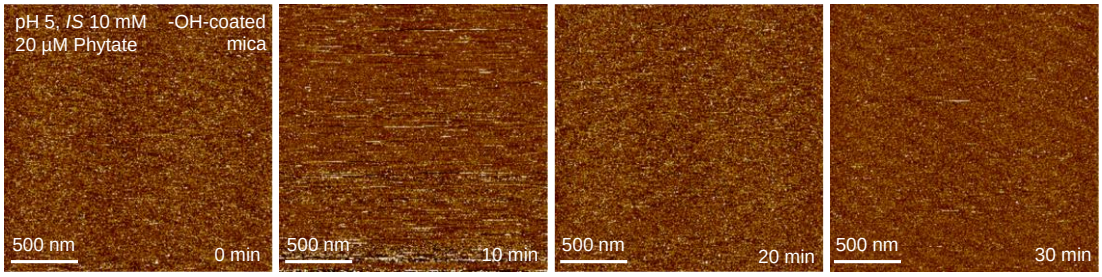

Fig. S19. No particles can be observed under the conditions of pH 5, *IS* = 10 mM containing 20 µM phytate on the -OH-coated mica.

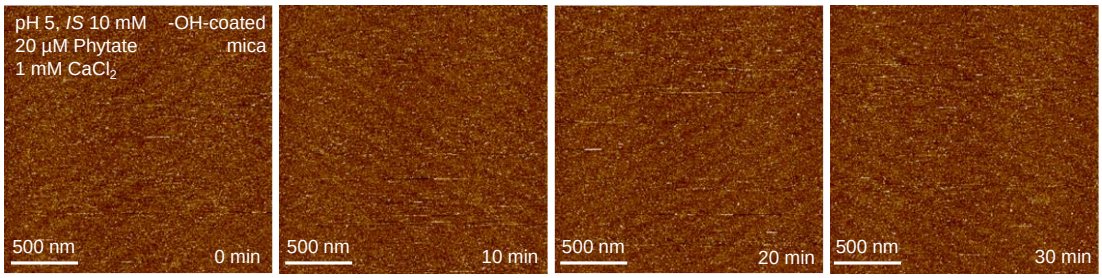

Fig. S20. No particles can be observed under the conditions of pH 5, *IS* = 10 mM containing 20 µM phytate and 1 mM $CaCl_2$ on the -OH-coated mica.

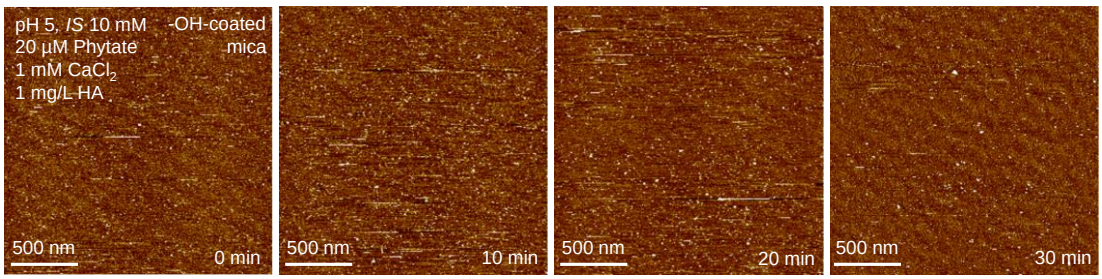

Fig. S21. No particles can be observed under the conditions of pH 5, *IS* = 10 mM containing 20 µM phytate, 1 mM $CaCl_2$ and 1 mg/L HA on the -OH-coated mica.

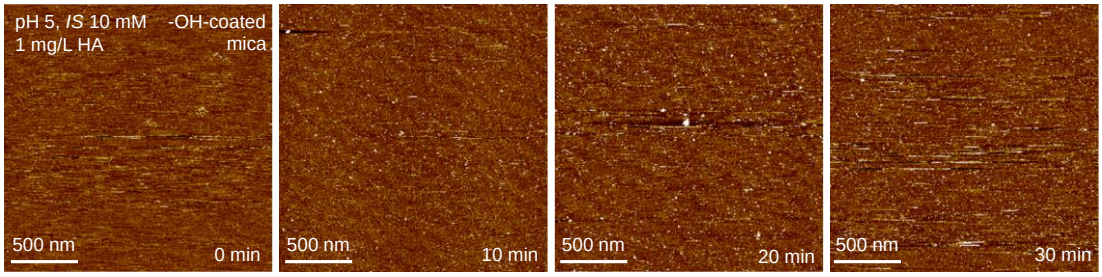

Fig. S22. No particles can be observed under the conditions of pH 5, *IS* = 10 mM containing 1 mg/L HA on the -OH-coated mica.

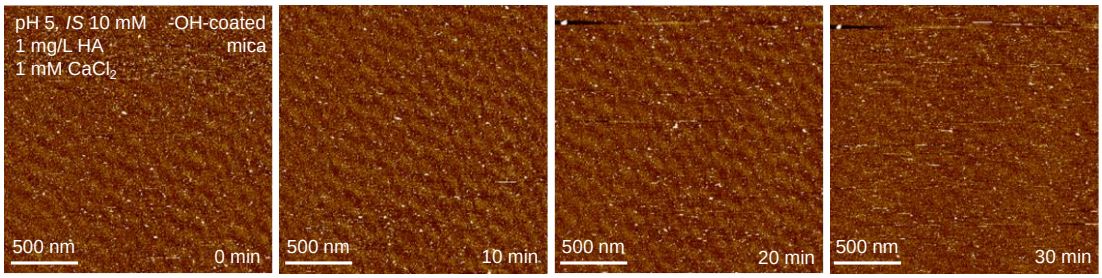

Fig. S23. No particles can be observed under the conditions of pH 5, *IS* = 10 mM containing 1 mg/L HA and 1 mM $CaCl_2$ on the -OH-coated mica.

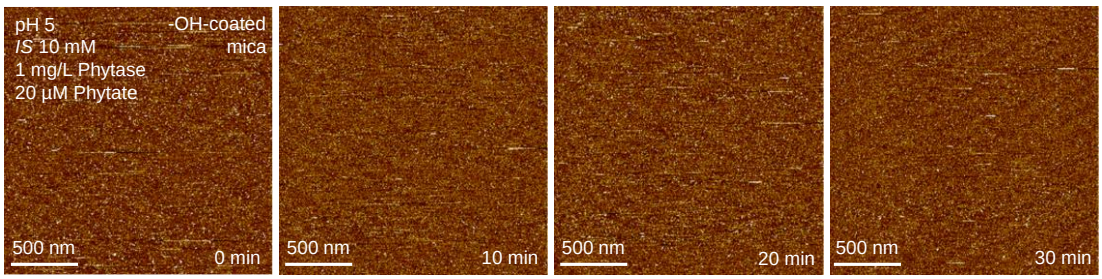

Fig. S24. No particles can be observed under the conditions of pH 5, *IS* = 10 mM containing 1 mg/L phytase and 20 µM phytate on the -OH-coated mica.

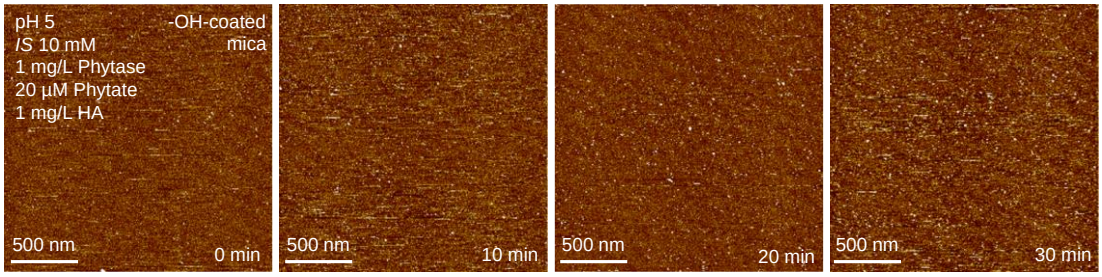

Fig. S25. No particles can be observed under the conditions of pH 5, *IS* = 10 mM containing 1 mg/L phytase, 20 µM phytate and 1 mg/L HA on the -OH-coated mica.

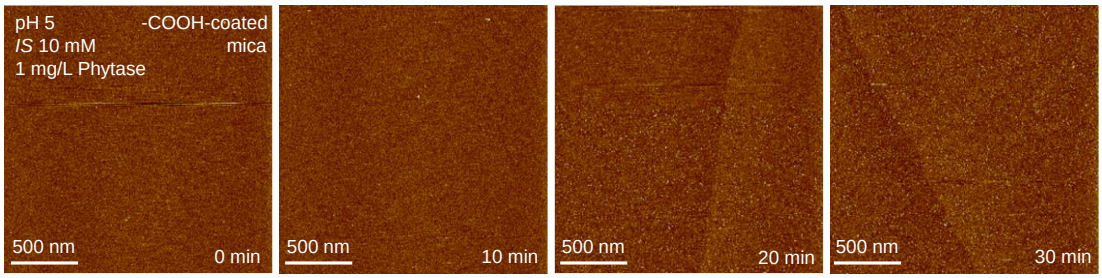

Fig. S26. No particles can be observed under the conditions of pH 5, *IS* = 10 mM containing 1 mg/L phytase on the -COOH-coated mica.

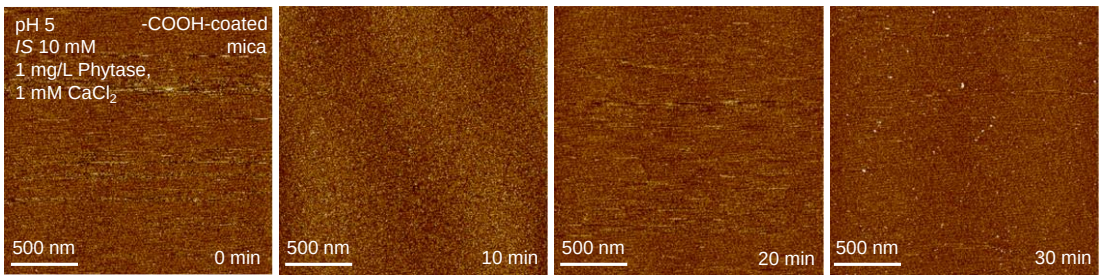

Fig. S27. No particles can be observed under the conditions of pH 5, *IS* = 10 mM containing 1 mg/L phytase and 1 mM $CaCl_2$ on the -COOH-coated mica.

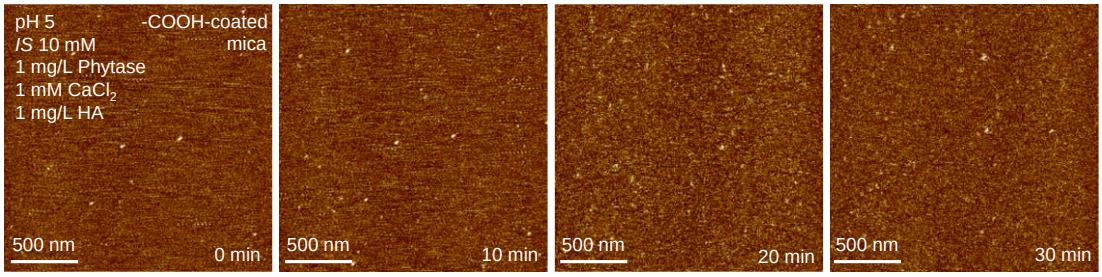

Fig. S28. No particles can be observed under the conditions of pH 5, *IS* = 10 mM containing 1 mg/L phytase, 1 mM $CaCl_2$ and 1 mg/L HA on the -COOH-coated mica.

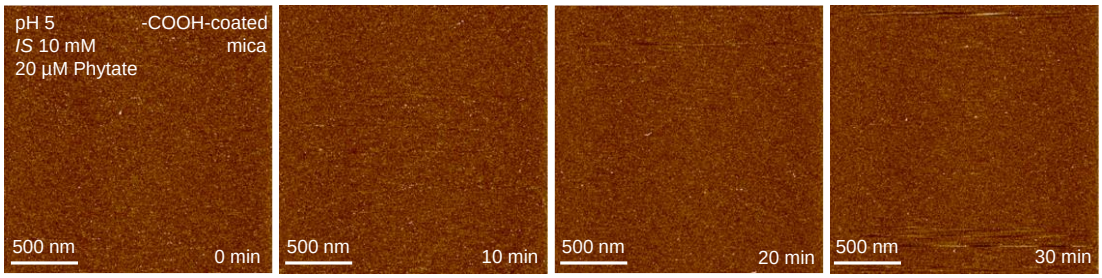

Fig. S29. No particles can be observed under the conditions of pH 5, *IS* = 10 mM containing 20 µM phytate on the -COOH-coated mica.

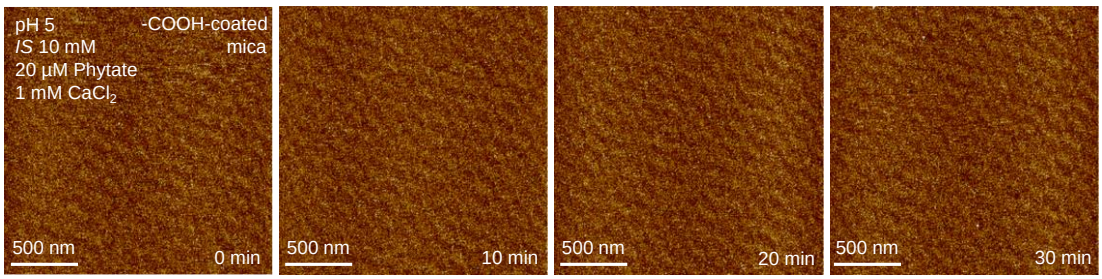

Fig. S30. No particles can be observed under the conditions of pH 5, *IS* = 10 mM containing 20 µM phytate and 1 mM $CaCl_2$ on the -COOH-coated mica.

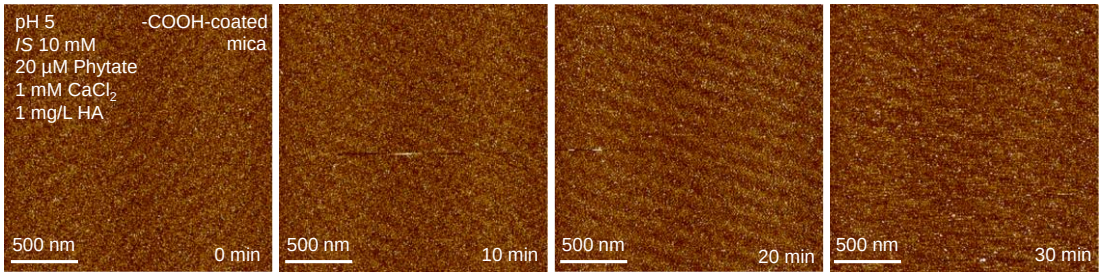

Fig. S31. No particles can be observed under the conditions of pH 5, *IS* = 10 mM containing 20 µM phytate, 1 mM $CaCl_2$ and 1 mg/L HA on the -COOH-coated mica.

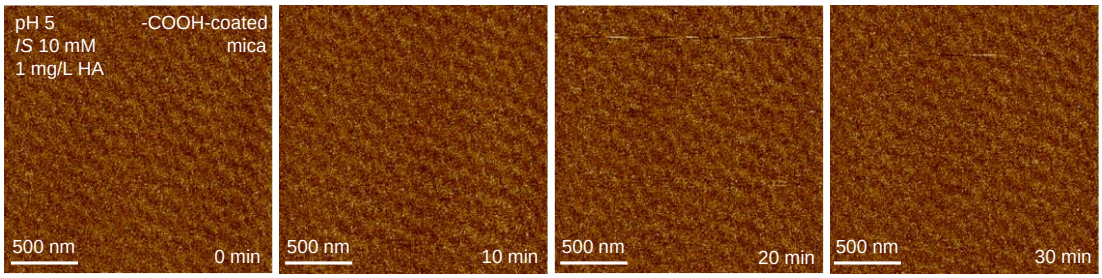

Fig. S32. No particles can be observed under the conditions of pH 5, *IS* = 10 mM containing 1 mg/L HA on the -COOH-coated mica.

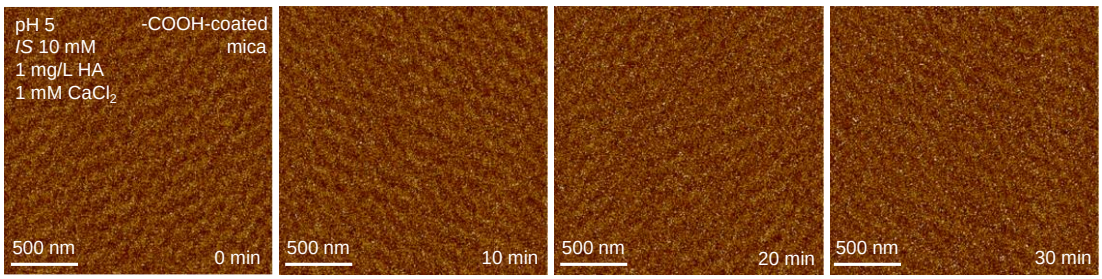

Fig. S33. No particles can be observed under the conditions of pH 5, *IS* = 10 mM containing 1 mg/L HA and 1 mM $CaCl_2$ on the -COOH-coated mica.

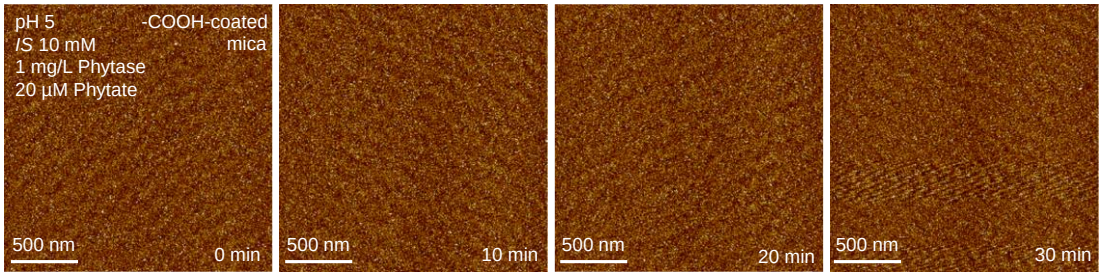

Fig. S34. No particles can be observed under the conditions of pH 5, *IS* = 10 mM containing 1 mg/L phytase and 20 µM phytate on the -COOH-coated mica.

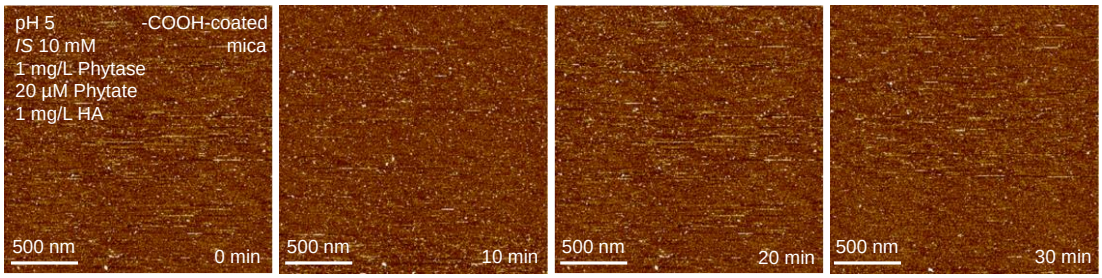

Fig. S35. No particles can be observed under the conditions of pH 5, *IS* = 10 mM containing 1 mg/L phytase, 20 µM phytate and 1 mg/L HA on the -COOH-coated mica.

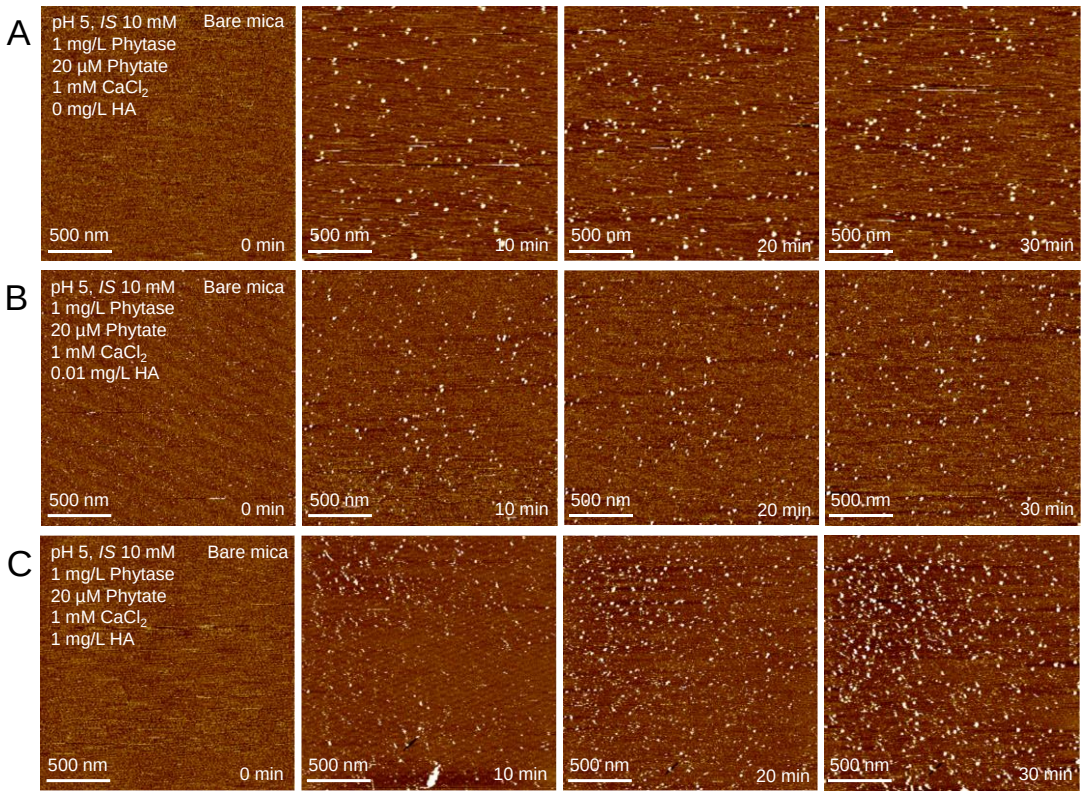

Fig. S36. AFM images of the particle nucleation with time on bare mica (001) in solutions containing 1 mg/L phytase, 20 µM phytate, 1 mM $CaCl_2$ (pH 5, *IS* = 10 mM) in (A) the absence and (B) presence of 0.01 and (C) 1 mg/L HA.

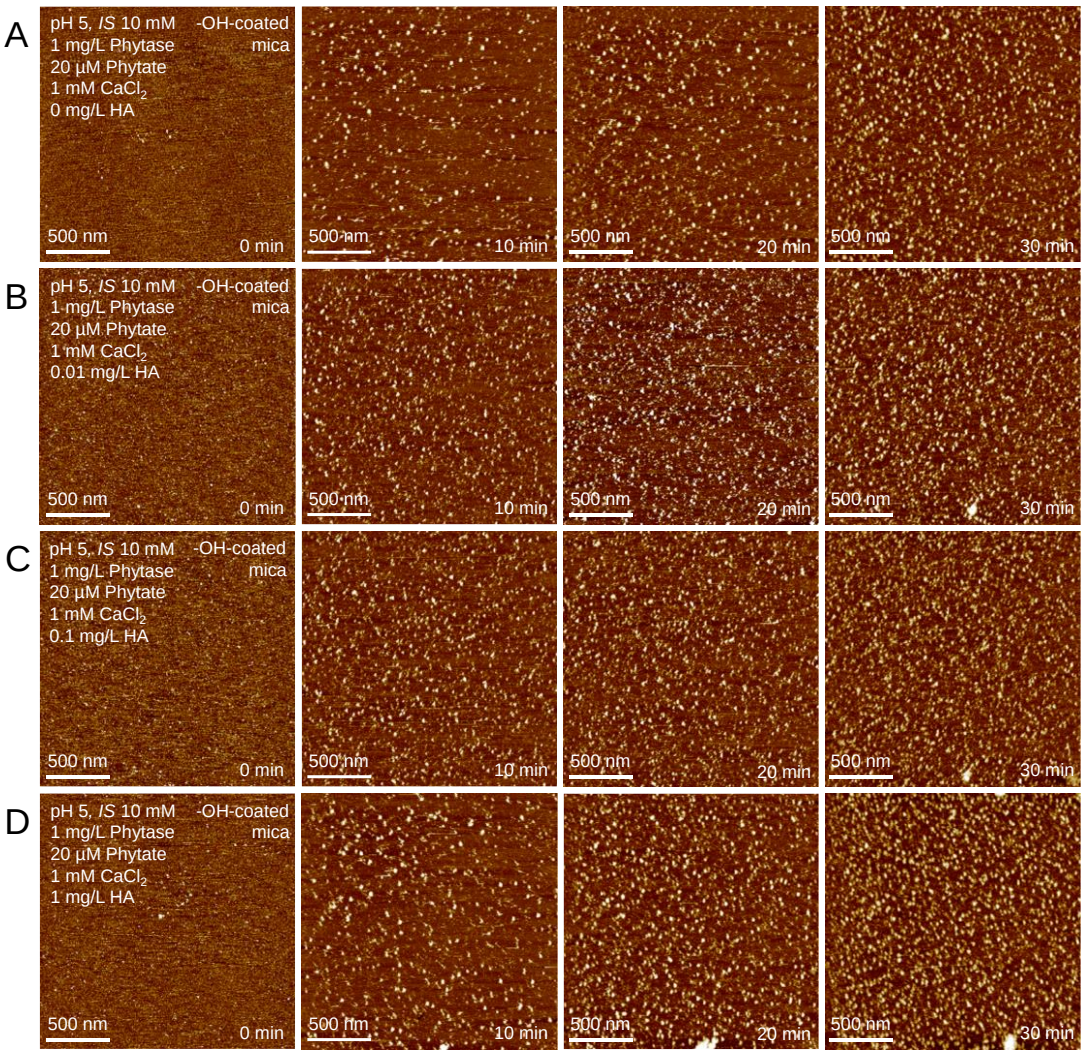

Fig. S37. AFM images of the particle nucleation with time on surfaces of –OH-coated mica (001) in solutions containing 1 mg/L phytase, 20 µM phytate, 1 mM $CaCl_2$ (pH 5, *IS* = 10 mM) in (A) the absence and (B-D) presence of HA ranging from 0.01 to 1 mg/L.

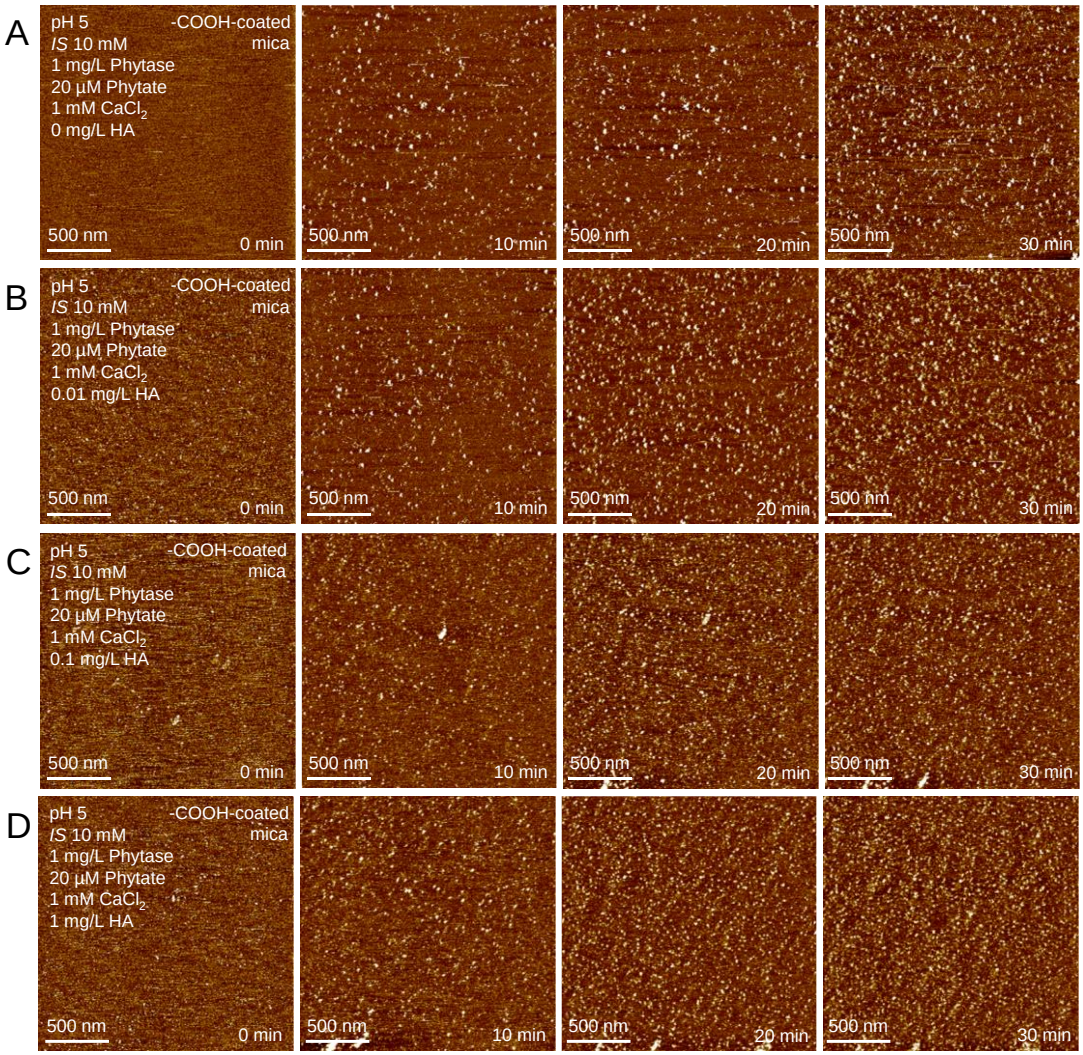

Fig. S38. AFM images of the particle nucleation with time on surfaces of –COOH-coated mica (001) in solutions containing 1 mg/L phytase, 20 µM phytate, 1 mM $CaCl_2$ (pH 5, *IS* = 10 mM) in (A) the absence and (B-D) presence of HA ranging from 0.01 to 1 mg/L.

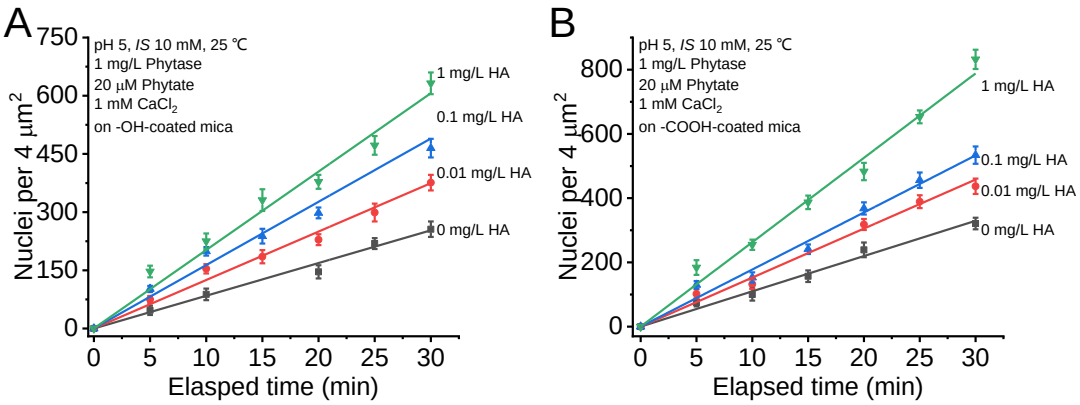

Fig. S39. The number of nucleated particles in solutions (1 mg/L phytase, 20 μM phytate, 1 mM $CaCl_2$, pH 5 and *IS* =10 mM) on surfaces of (A) -OH-coated and (B) -COOH-coated mica, increases linearly over elapsed time. The nucleation rate increases with the increase of HA concentrations ranging from 0.01 to 1 mg/L.

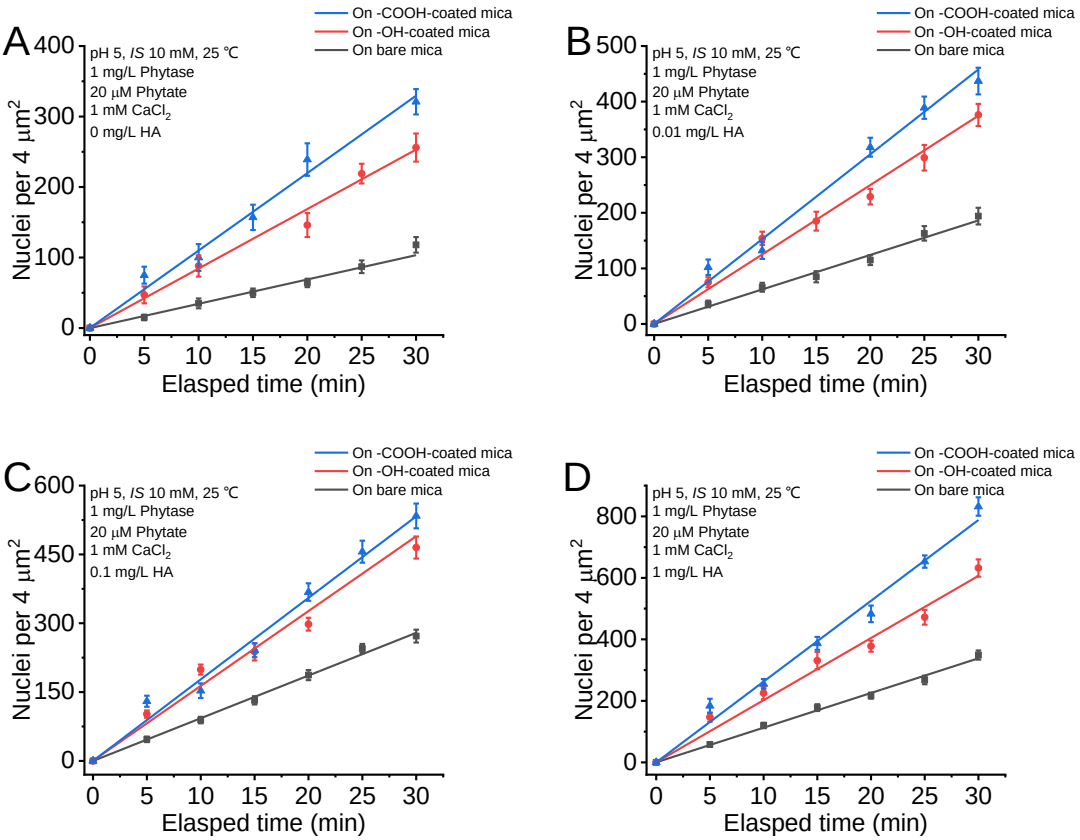

Fig. S40. The number of the nucleated particles in solutions (1 mg/L phytase, 20 μM

phytate, 1 mM $CaCl_2$, pH 5 and *IS* =10 mM) in (A) the absence and (B-D) presence of HA ranging from 0.01-1 mg/L on surfaces of bare, -OH-coated or -COOH-coated mica, increases linearly over elapsed time.

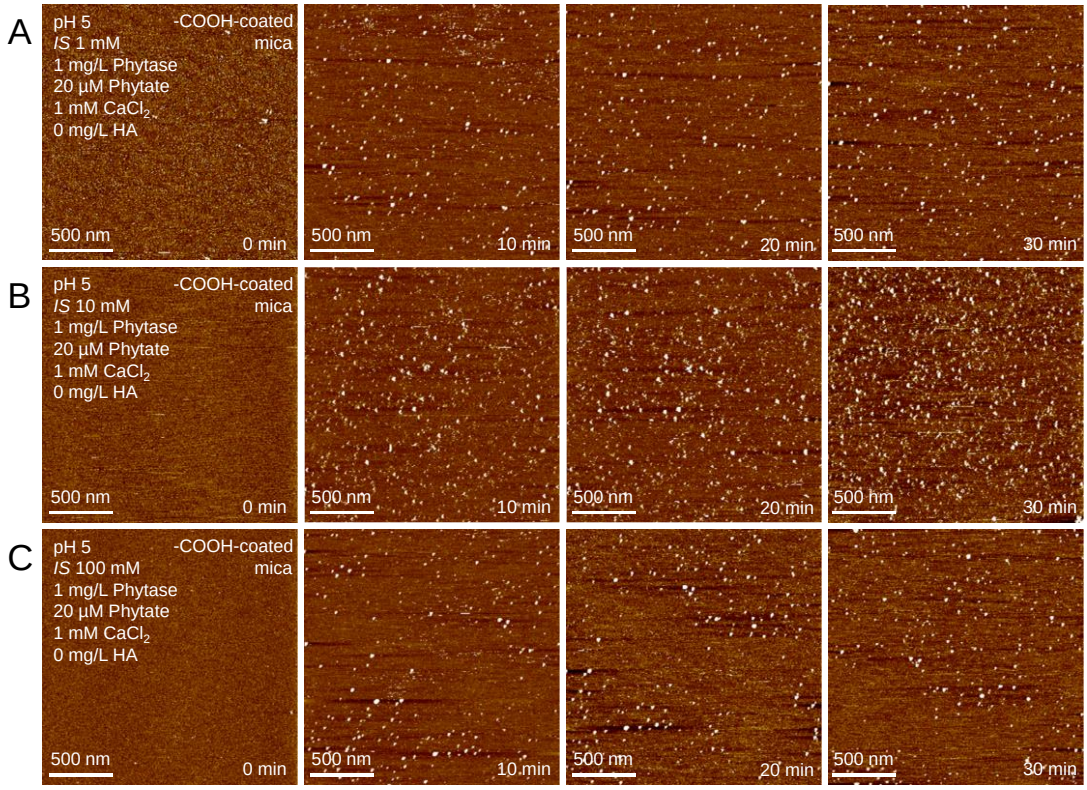

Fig. S41. AFM images of the particle nucleation with time on -COOH-coated mica surfaces (001) in solutions containing 1 mg/L phytase, 20 µM phytate, 1 mM $CaCl_2$ and pH 5) in the absence of HA with *IS* at (A) 1, (B) 10 and (C) 100 mM, respectively.

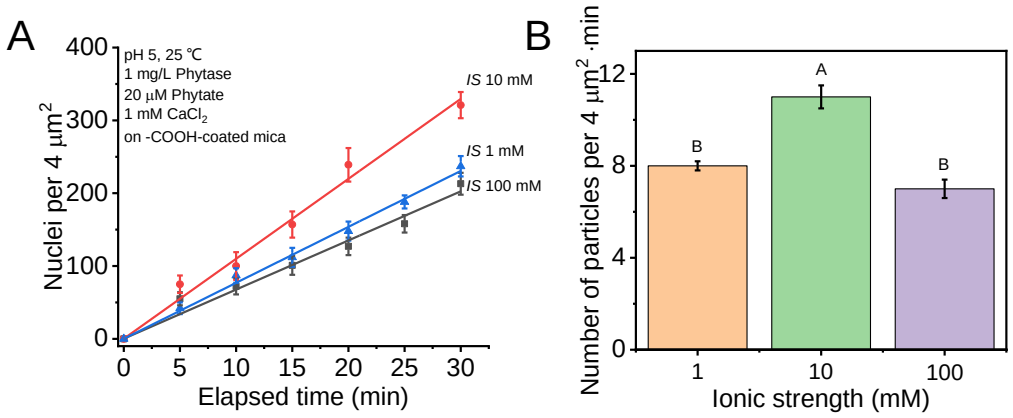

Fig. S42. (A) The number of nucleated particles increases linearly with time on surfaces of-COOH-coated mica. (B) Significance analyses of nucleation rates at different ionic strengths. Uppercase letters indicate a significant difference at $P < 0.01$, which analyzed by SPSS software.

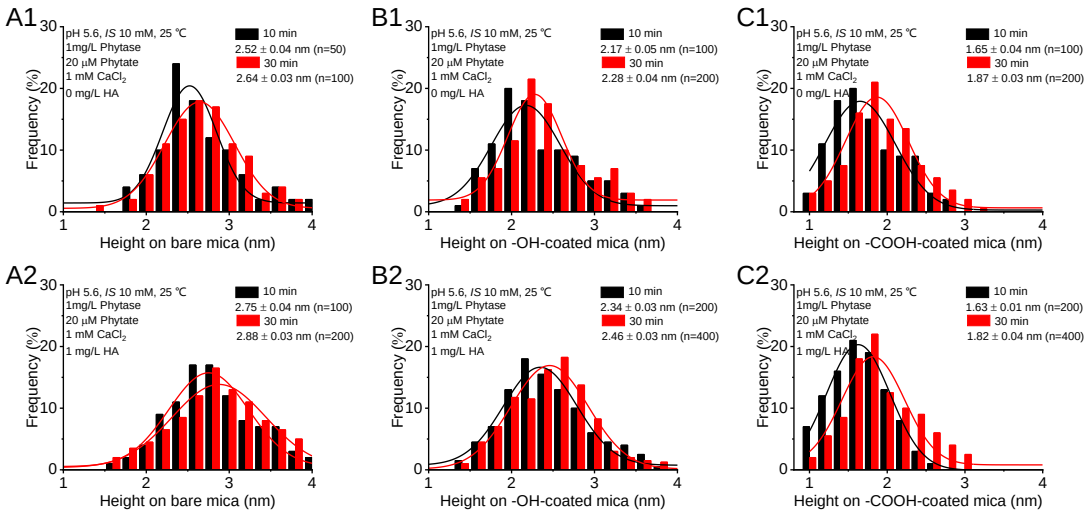

Fig. S43. Size distributions of particles (in height measure by AFM) nucleated on surfaces of (A) bare, (B) -OH and (C) -COOH-coated mica in the absence and presence of 1mg/L HA.

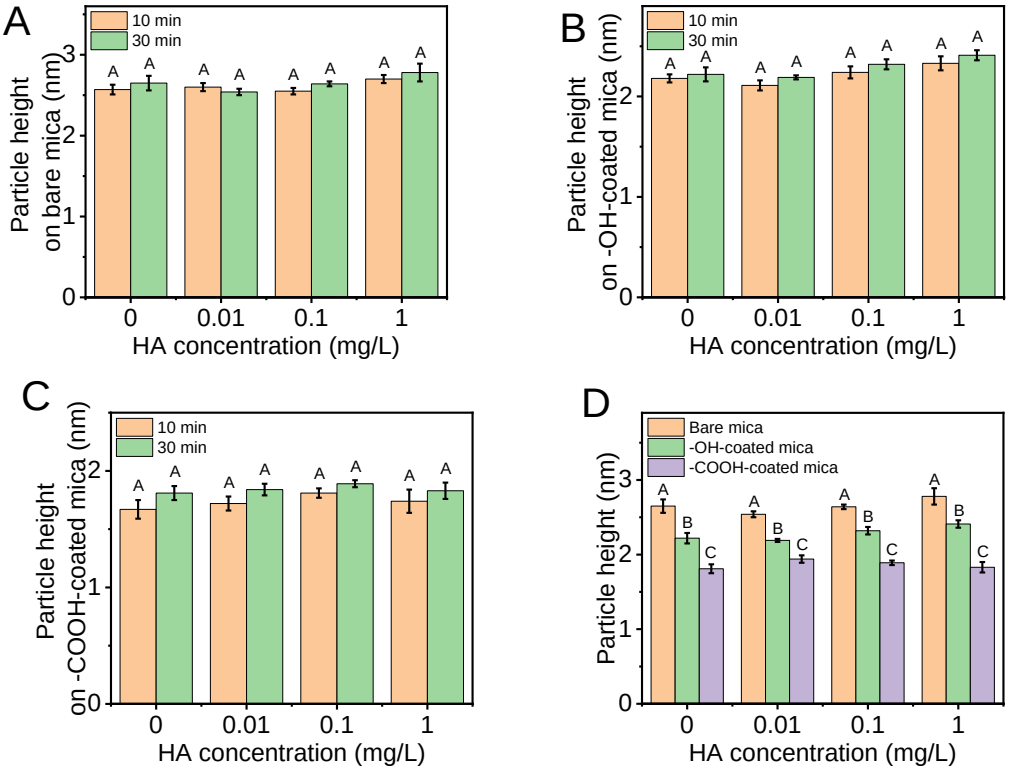

Fig. S44. Significance analyses of the height of particles on nucleation surfaces of (A) bare (B) -OH- and (C) -COOH-coated mica at 10 and 30 min, respectively, in the absence and presence of HA ranging from 0.01-1 mg/L, showing the particle height remains relatively constant. This indicates that nucleation rather than particle growth predominates during the precipitation time of 30 min. (D) Significance analyses of particle heights on different surfaces of mica in the absence and presence of HA ranging from 0.01-1 mg/L demonstrating that organically-coated surfaces can enhance the nucleation rate. Different uppercase letters indicate significant difference at $P <$ 0.01, which was analyzed by SPSS software.

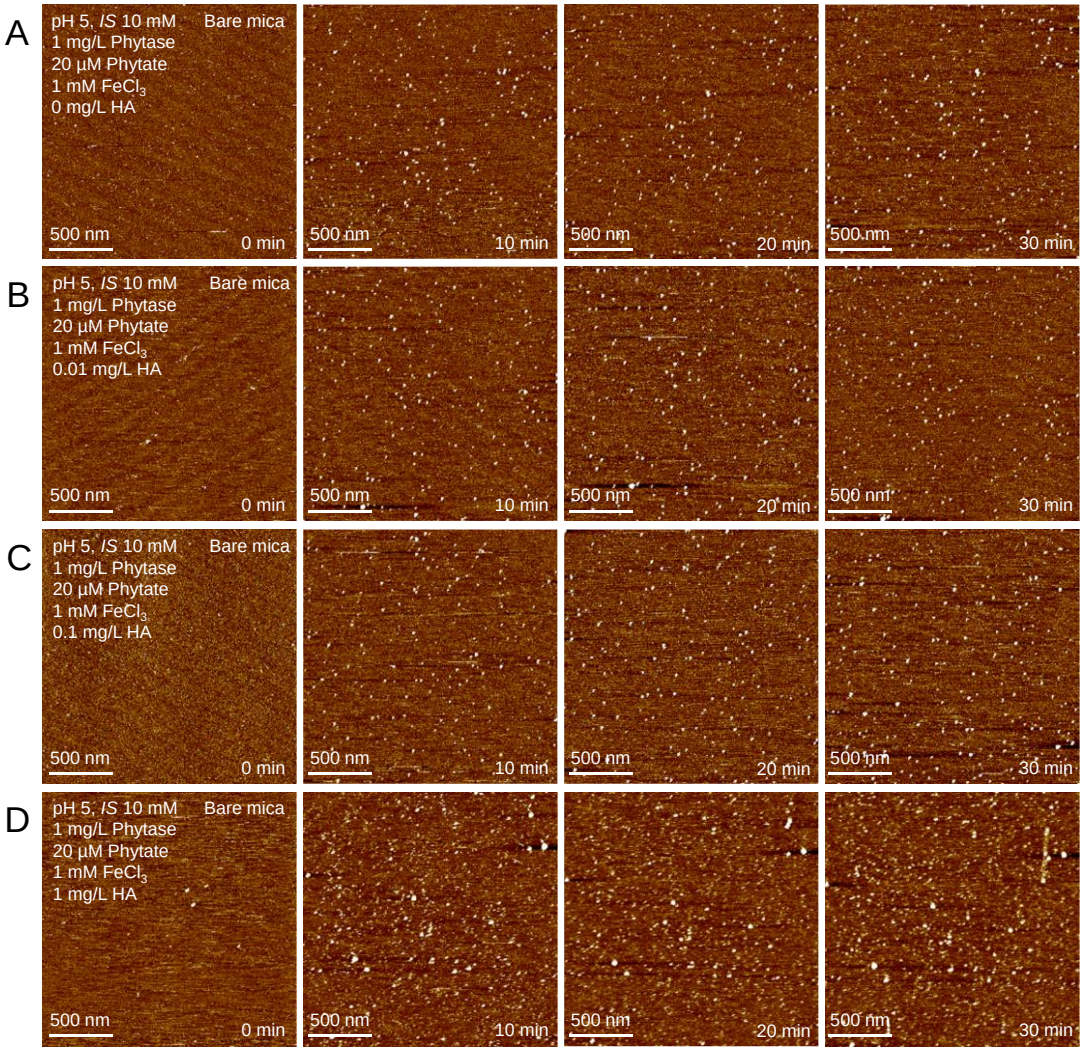

Fig. S45. AFM images of the particle nucleation with time on surfaces of bare mica (001) in solutions containing 1 mg/L phytase, 20 µM phytate, 1 mM $FeCl_3$ (pH 5, *IS* = 10 mM) in (A) the absence and (B-D) presence of HA ranging from 0.01 to 1 mg/L.

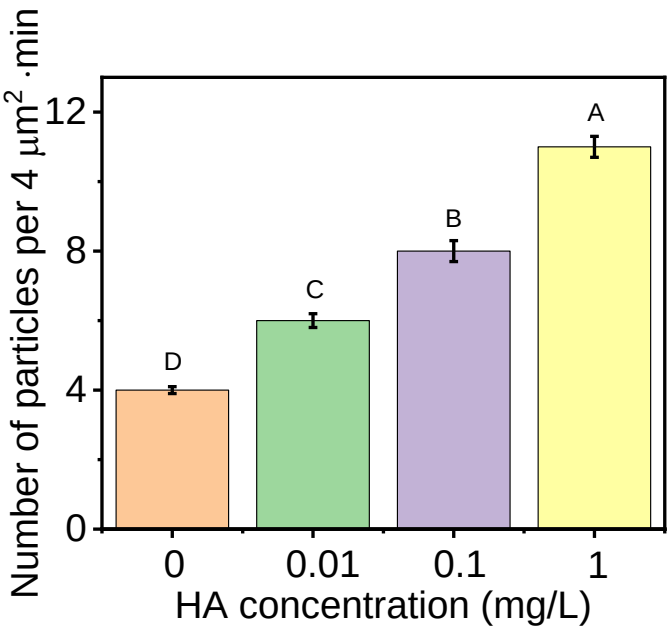

Fig. S46. Significance analyses of nucleation rates at different concentrations of HA on bare mica. Uppercase letters indicate a significant difference at $P < 0.01$, which was analyzed by SPSS software.

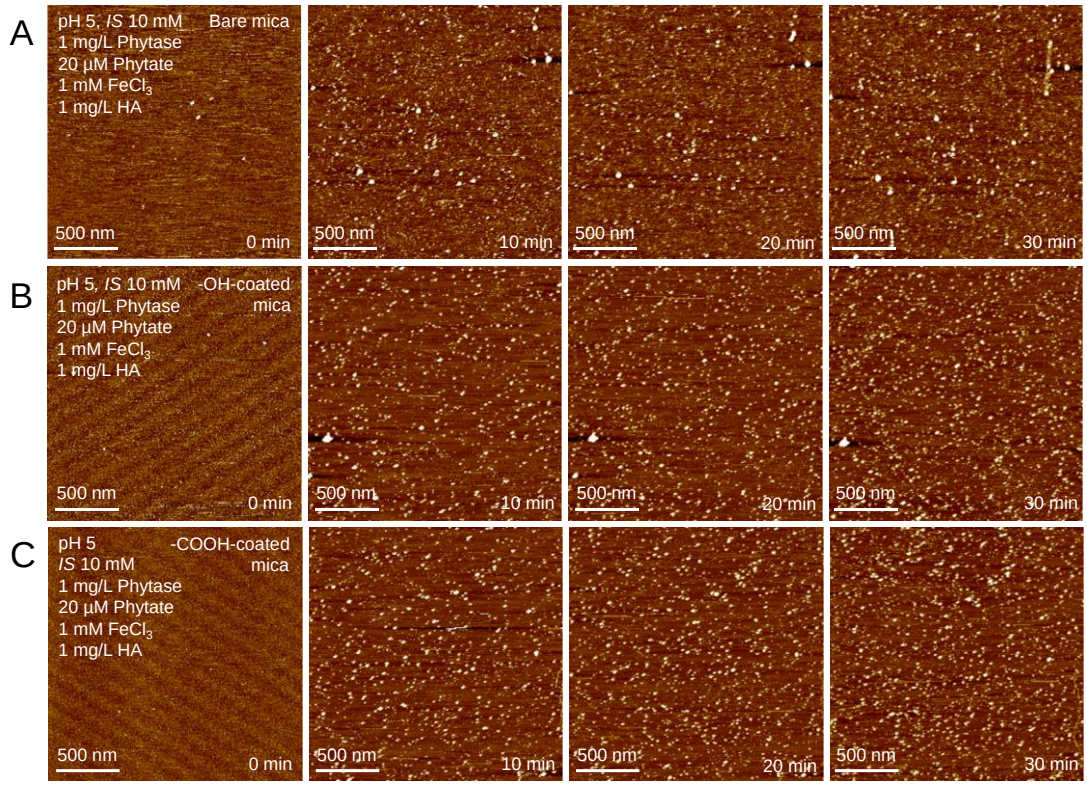

Fig. S47. AFM images of the particle nucleation with time in solutions (1 mg/L phytase, 20 μM phytate, 1 mM $CaCl_2$, pH 5 and *IS* =10 mM) on surfaces of (A) bare, (B) -OH- and (C) -COOH-coated mica in the presence of 1 mg/L HA.

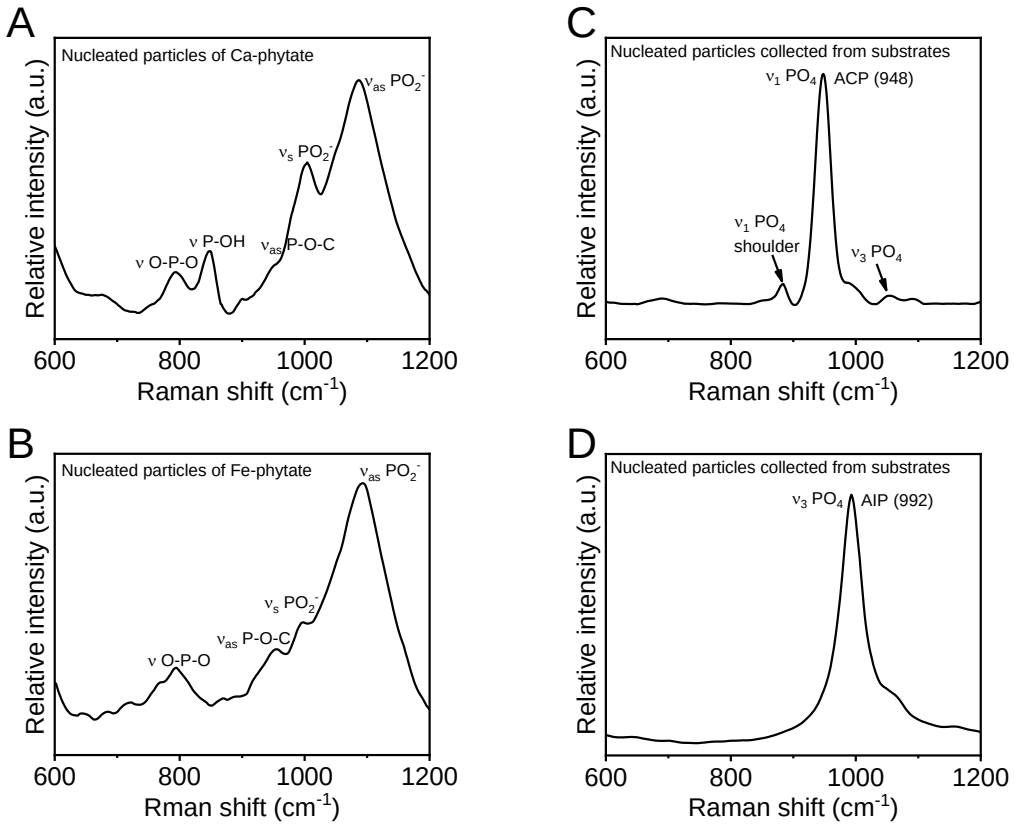

Fig. S48. (A, B) Raman spectra of Ca/Fe-phytate complexes. The Raman characteristic peaks of Ca/Fe-phytate have been identified and and bands of $\nu_s\ PO_2^-$ and $\nu_{as}\ PO_2^-$ have been considered as direct Ca/Fe-O-P coordination. (C, D) Raman spectra of the nucleated particles collected from both bare and organically-coated mica surfaces. The characterization of $\nu_1\ PO_4$ band (948 cm^{-1}) and $\nu_3\ PO_4$ band (992 cm^{-1}) indicated that particles were amorphous Ca-P_i and Fe-P_i, respectively, which were completely different from the Raman characteristic peaks of Ca/Fe-phytate

complexes.

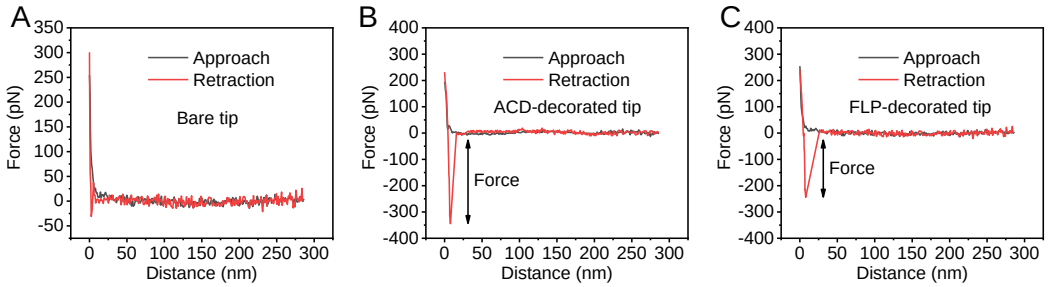

Fig. S49. Representative force curves obtained from the (A) bare tip, (B) ACD-decorated tip and (C) FLP-decorated tip on the HA particles deposited on bare mica surface.

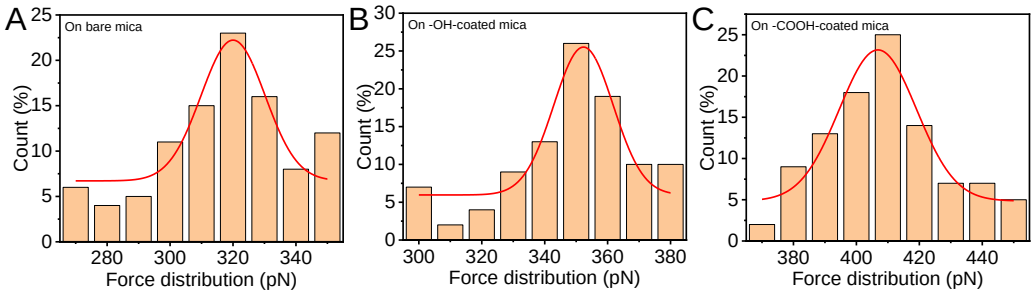

Fig. S50. Adhesion force distributions derived from PF-QNM-based adhesion force maps between ACD in phytase and HA deposited on surfaces of (A) bare, (B) -OH- and (C) -COOH-coated mica in solutions of pH 5 and *IS* = 10 mM.

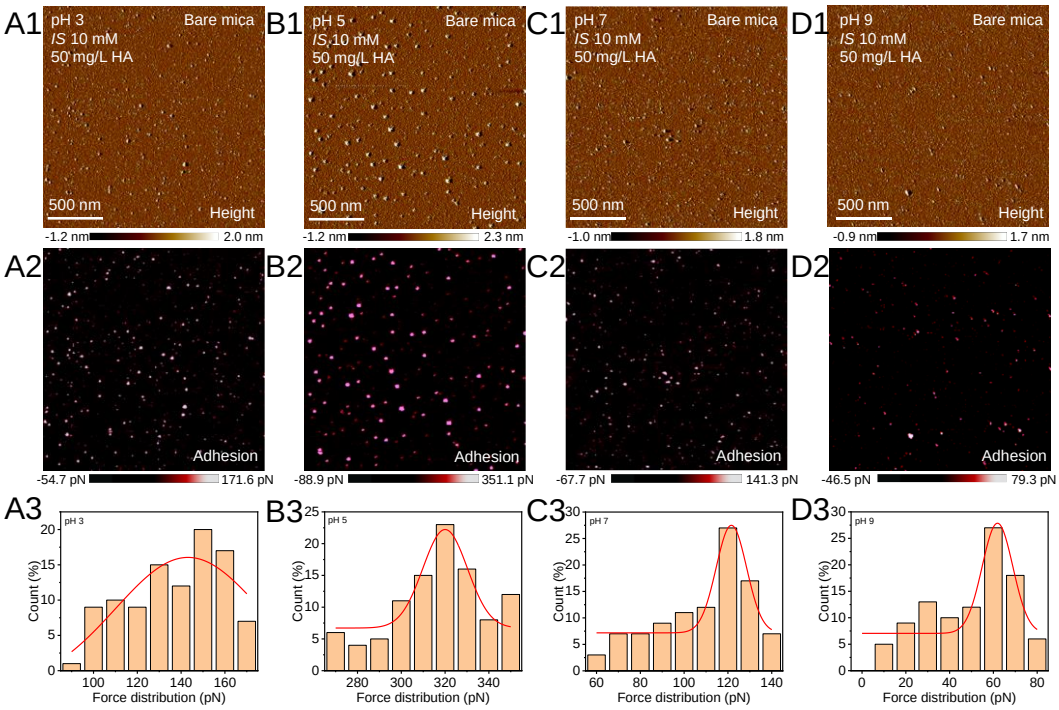

Fig. S51. Adhesion force distributions derived from PeakForce-QNM-based adhesion force maps between ACD in phytase and HA deposited on surfaces of mica in solutions of *IS* = 10 mM with different pH values of (A) 3, (B) 5, (C) 7 or (D) 9.

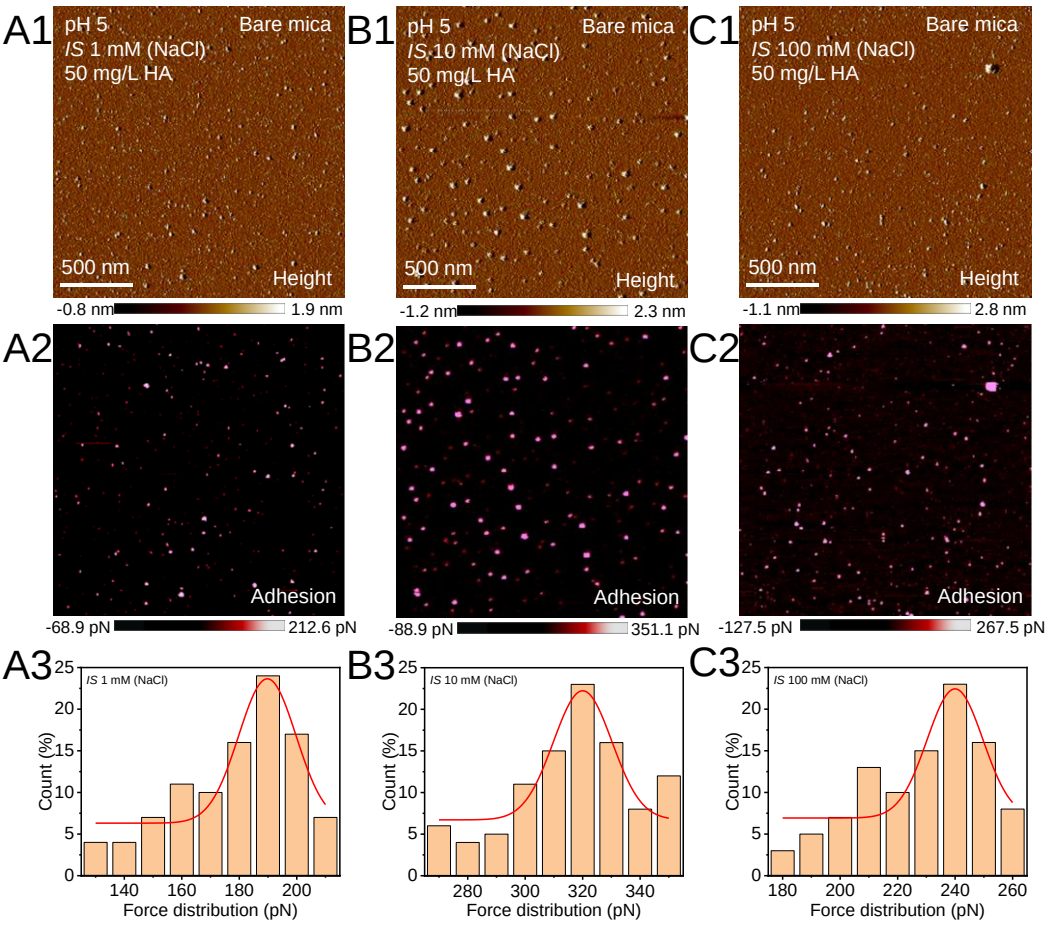

Fig. S52. Adhesion force distributions derived from PeakForce QNM-based adhesion force maps between ACD in phytase and HA deposited on surfaces of mica in solutions of pH 5 with different *IS* values of (A) 1, (B) 10, and (C) 100 mM adjusted by NaCl.

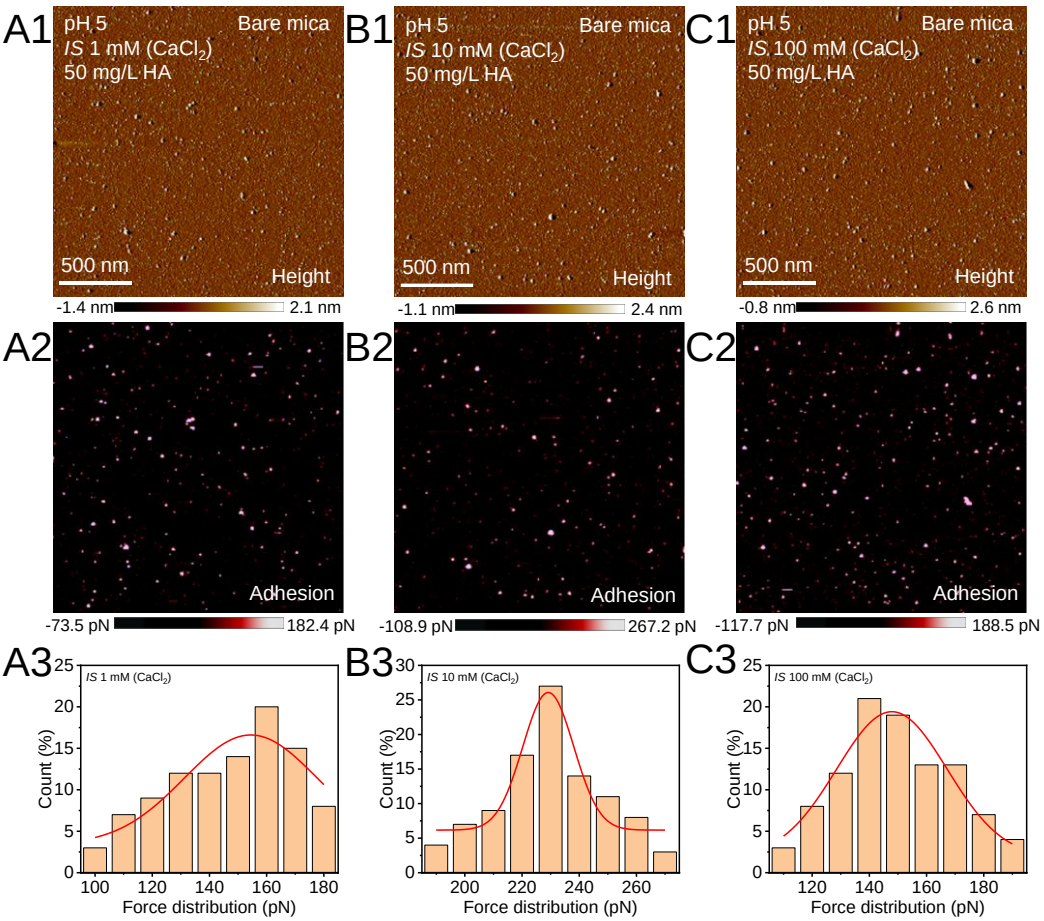

Fig. S53. Adhesion force distributions derived from PeakForce-QNM-based adhesion force maps between ACD in phytase and HA deposited on surfaces of mica in solutions of pH 5 with different *IS* values of (A) 1, (B) 10, and (C) 100 mM adjusted by $CaCl_2$.

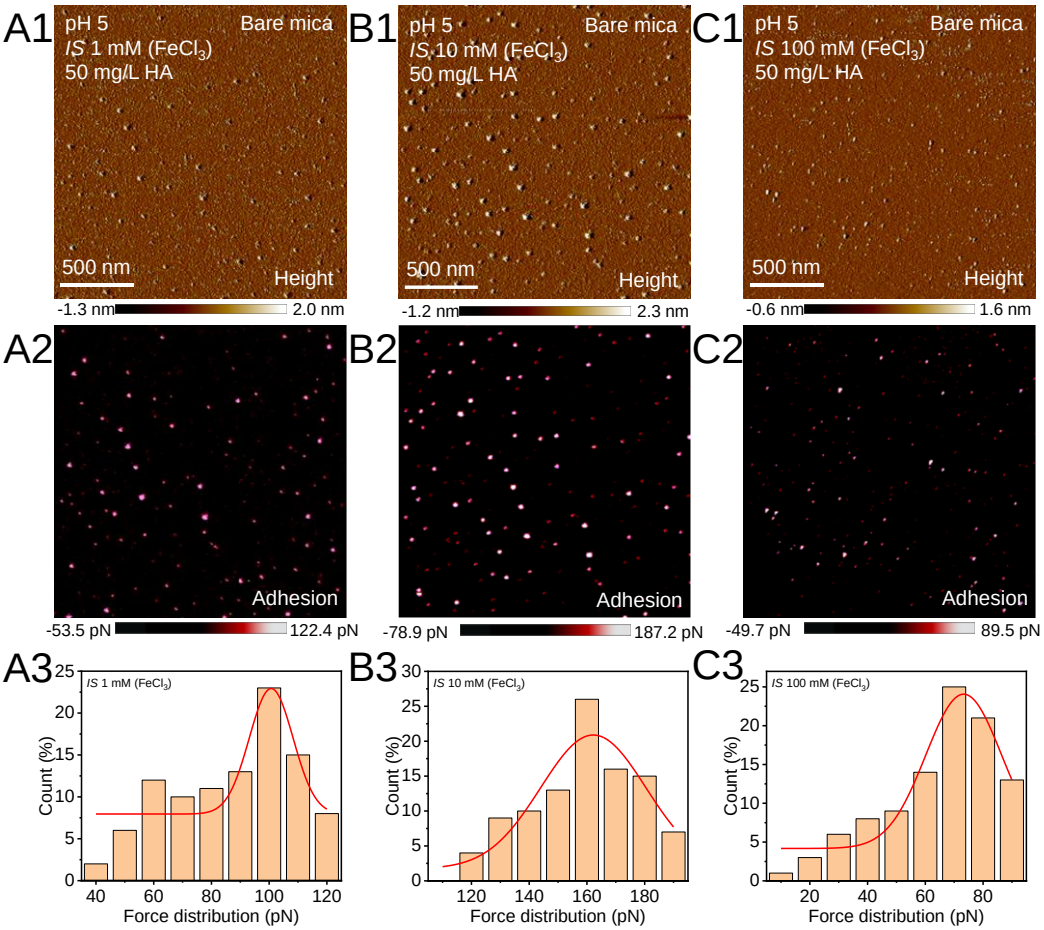

Fig. S54. Adhesion force distributions derived from PeakForce-QNM-based adhesion force maps between ACD in phytase and HA deposited on surfaces of mica in solutions of pH 5 with different *IS* values of (A) 1, (B) 10, and (C) 100 mM adjusted by $FeCl_3$.

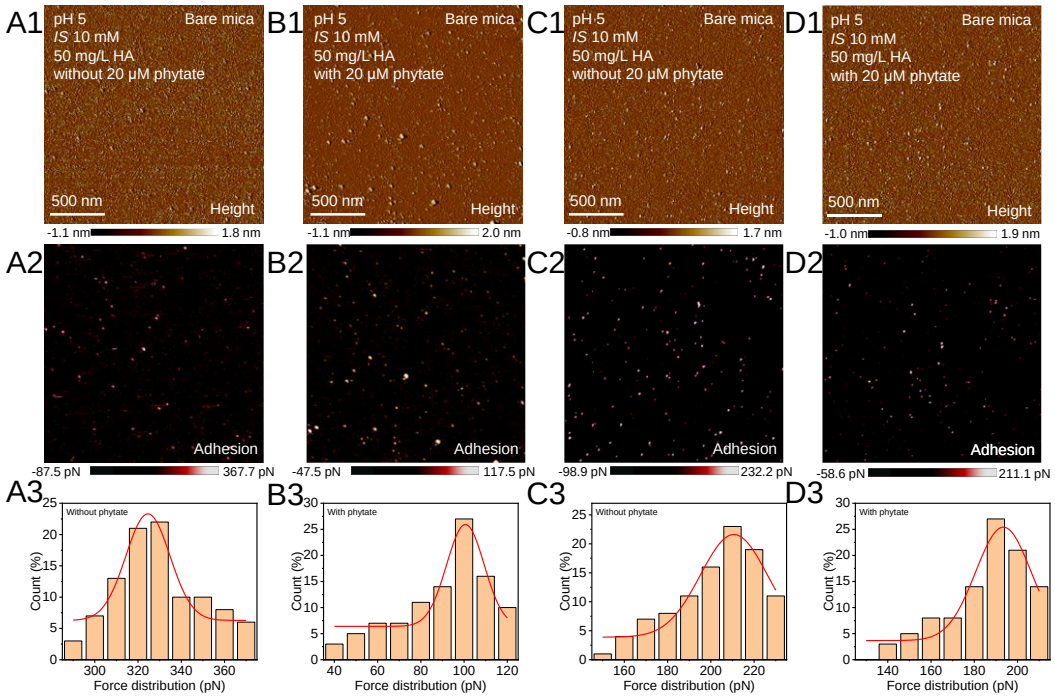

Fig. S55. Adhesion force distributions derived from PeakForce-QNM-based adhesion force maps between (A-B) an active catalytic domain (ACD) in phytase or (C-D) full-length phytase (FLP) and HA deposited on surfaces of mica in solutions of pH 5 and *IS* = 10 mM in the absence and presence of phytate.

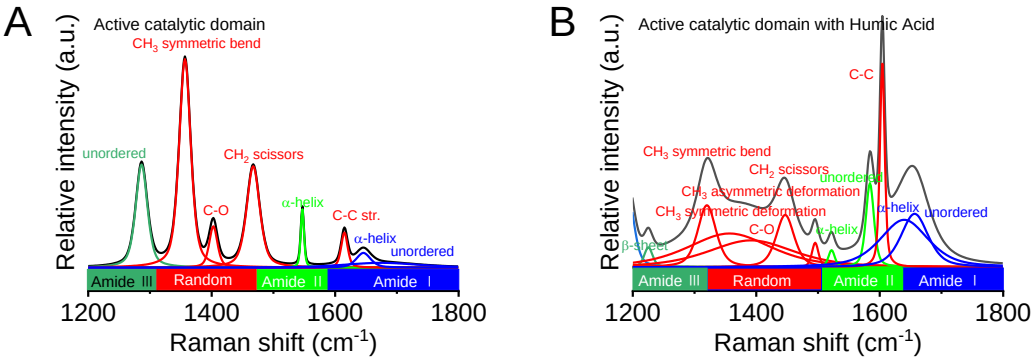

Fig. S56. Fitting Raman spectra of secondary structures of ACD in phytase at 100 mg/L in solutions (pH 5 and *IS* = 10 mM) in (A) the absence and (B) presence of 1 mg/L HA.

SI References

1 W. Tan, J. Xiong, Y. Li, M. Wang, L. Weng and L. K. Koopal, Proton binding to soil humic and fulvic acids: experiments and NIC-Donnan modeling. *Colloids Surf. A Physicochem. Eng. Asp*., 2013, **436**, 1152– 1158.

2 W. Poel, S. Pintea, J. Drnec, F. Carla, R. Felici, P. Mulder, J. A. A. W. Elemans, W. J. P. van Enckevort, A. E. Rowan and E. Vlieg, Muscovite mica: flatter than a pancake, *Surf. Sci.,* 2014, **619**, 19-24.

3 Z. Wei, C. Wang and C. Bai, Investigation of nanoscale frictional contact by friction force microscopy, *Langmuir,* 2001, **17**, 3945-3951.

4 L. L. Wang, L. F. Wang, X. M. Ren, X. D. Ye, W. W. Li, S. J. Yuan, M. Sun, G. P. Sheng, H. Q. Yu and X. K. Wang, pH dependence of structure and surface properties of microbial EPS, *Environ*. *Sci*. *Technol*., 2012, **46**, 737-744.

5 M. Keiluweit, J. J. Bougoure, P. S. Nico, J. Pett-Ridge, P. K. Weber and M. Kleber, Mineral protection of soil carbon counteracted by root exudates, *Nat. Clim. Change,* 2015, **5**, 588−595.

6 C. Dai, J. Zhao, D. E. Giammar, J. D. Pasteris, X. Zuo and Y. Hu, Heterogenous lead phosphate nucleation at organic-water interfaces: implications for lead immobilization, *ACS Earth Space Chem*., 2018, **2**, 869-877.

7 L. S. Shlyakhtenko, A. A. Gall and Y. L. Lyubchenko, Mica functionalization for imaging of DNA and protein-DNA complexes with atomic force microscopy,

Methods Mol. Biol., 2013, **931**, 295-312.

8 X. Ge, L. Wang, W. Zhang and C. V. Putnis, Molecular understanding of humic-limited phosphate precipitation and transformation, *Environ. Sci. Technol.,* 2020, **54**, 207-215.

9 R. W. Friddle, K. Battle, V. Trubetskoy, J. Tao, E. A. Salter, J. Moradian-Oldak, J. J. De Yoreo and A. Wierzbicki, Single-molecule determination of the face-specific adsorption of amelogenin's C terminus on hydroxyapatite, *Angew. Chem. Int. Ed*., 2011, **50**, 7541−7545.

10 J. Tao, K. C. Battle, H. Pan, E. A. Salter, Y. C. Chien, A. Wierzbicki and J. J. De Yoreo, Energetic basis for the molecular-scale organization of bone, *Proc. Natl. Acad. Sci. U. S. A.,* 2015, **112**, 326−331.

11 C. A. J. Putman, B. G. De Grooth, N. F. Van Hulst and J. Greve, A detailed analysis of the optical beam deflection technique for use in atomic force microscopy, *J. Appl. Phys.,* 1992, **72**, 6-12.

12 N. A. Burnham, X. Chen, C. S. Hodges, G. A. Matei, E. J. Thoreson, C. J. Roberts, M. C. Davies and S. J. B. Tendler, Comparison of calibration methods for atomic-force microscopy cantilevers, *Nanotechnology,* 2003, **14**, 1-6.

13 J. Murphy and J. P. Riley, A modified single solution method for the determination of phosphate in natural waters, *Anal. Chim. Acta,* 1962, **27**, 31-36.

14 S. Cai and B. R. Singh, Identification of β-turn and random coil amide III infrared bands for secondary structure estimation of proteins, *Biophys. Chem.* 1999, **80**, 7–20.

15 S. Elsharkawy, M. Al-Jawad, M. F. Pantano, E. Tejeda-Montes, K. Mehta, H. Jamal and R. M. Wilson, Protein disorder−order interplay to guide the growth of hierarchical mineralized structures, *Nat. Commun.* 2018, **9**, 2145.